This project has received funding from the European Union's Horizon 2020 research and innovation programme under grant agreement No 727616.

Biofficiency

Performance of tests in lab-scale test rig (D4.1)

Author:	Flemming Jappe Frandsen, Jesper Thor Funch, Semira Naimi, Guoliang Wang, Pedro Abelha, Peter Arendt Jensen, Simon Leiser
Version:	Final
Quality Review:	Sebastian Fendt
Date:	09.09.2019
Partners involved:	DTU, TNO

Grant Agreement No.	727616
Starting Date:	01.11.2016
Duration:	36 months

Disclaimer

The content of this deliverable does not reflect the official opinion of the European Commission. Responsibility for the information and views expressed herein lies entirely with the author(s).

Table of Contents

Abbreviations and Acronyms

CFA	Coal fly ash
CHP	Combined Heat and Power
D	Deliverable
EDX	Energy-dispersive X-ray spectroscopy
EFR	Entrained flow reactor
HDP	Horizontal deposition probe
HTC	Hydrothermal carbonization
ICP	Inductively coupled plasma
LCS	Lab-scale combustion simulator
PF	Pulverised Fuel
SE	Steam explosion
SEM	Scanning electron microscopy
TGA	Thermogravimetric analysis
WP	Work package
XK	Potassium conversion
XRD	X-ray diffraction

Introduction

Utilization of energy from biomass in Germany began in small [< 20 MWth] dedicated Combined Heat and Power (CHP) plants, typically based on grate-firing technology, or in some cases on fluidized bed technology. Thermal processing of e.g. straw or wood chips in small plants is possible, but it does require a significant number of plants to process a significant amount of biomass, and often the thermal processing is associated with some rather serious operational problems, i.e. slagging, fouling and corrosion in grate-fired units, and, de-fluidization in FBC-units [Frandsen, 2011].

Then it was suggested to shift strategy, and co-fire biomass with coal in PC-fired units. These plants are much bigger [< 600 MWth] than the grate-fired units, and at the same time have a much higher electrical efficiency, up to 48 %, compared to ~ 30 % for the grate fired units, see *Figure 1*.

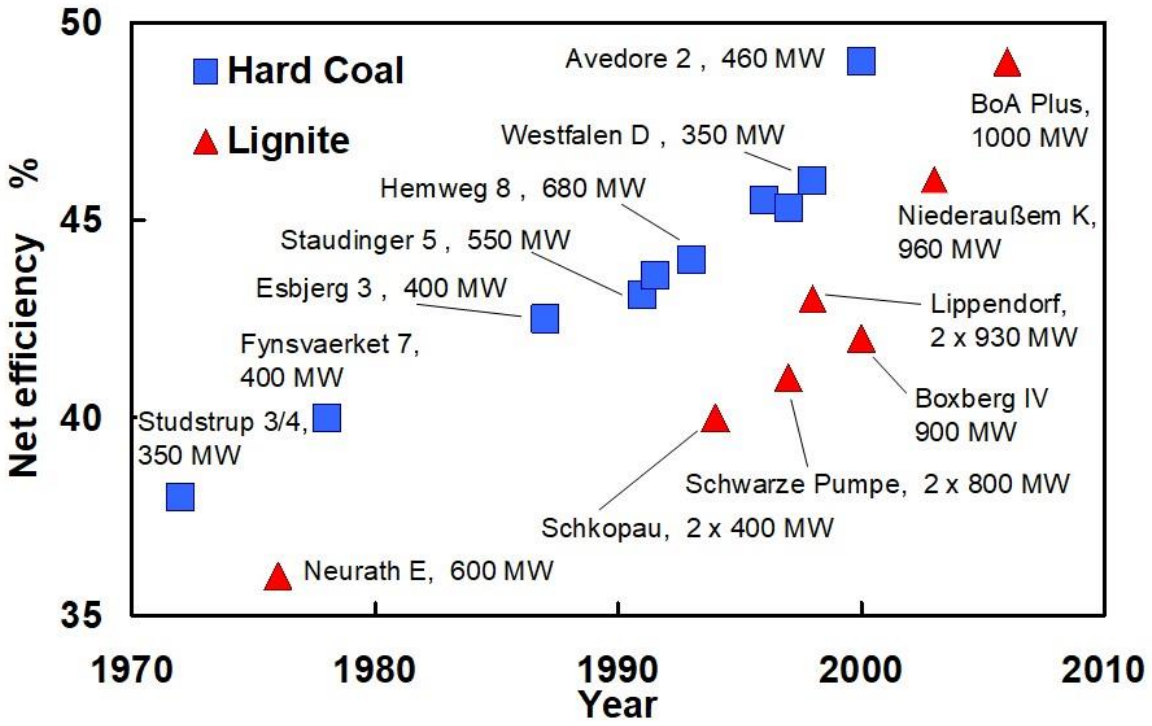

Figure 1: Development in electrical efficiency for PC-fired units, in the period 1970-2010. Source: [Hein, 2008].

Thus, by using PC-fired units, a much higher amount of biomass could be processed at a much higher electrical efficiency. Many technical problems were solved in relation to this development, and as part of the massive demo program at the Midtkraft Studstrup power Station in Denmark, it was shown that it is possible to co-fire <17 % high-K wheat straw with coal, provided that the coal has a high ash quality, rich in Al and Si, which acts as a binder for the high levels of K, released from the straw during processing [Frandsen, 2011].

The natural continuation of the development would be to process biomass thermally, alone, in PF-fired units, as so-called biodust. But there is a catch to this, since the biomass, being either wood or straw pellets do not contain enough ash to fix the significant amount of K, present in biomass. Thus, an additive is needed to act as a drain for the K, by interacting with K in the gas phase, thereby releasing Cl and HCl(g), and preventing K from forming low-melting, sticky phases which may deposit [Frandsen, 2011].

Recently, a lot of focus has been put into testing all kinds of solid residues rich in Al and Si, or S and Ca/P. This is also one of the subjects of Biofficiency WP4.

WP4 deals with both pilot-scale measurements of deposits (at DTU) [Task 4.1.], small-particle formation (at TUM) [Task 4.2.], as well as full-scale deposition and small-particle measurements at two Danish power stations (by DONG/Ørsted, DTU and TUM) [Task 4.3.].

In the time between the preparation, and the granting, of the Biofficiency application, the DTU Entrained Flow Reactor (EFR), was heavily applied on investigations of ash and deposit formation, in pulverized fuel-fired systems.

[Damoe et al., 2017] carried out combustion experiments with pulverized biomass fuels (two straw fuels, and two wood fuels), in the EFR at 1200−1400 °C, simulating full-scale suspension-firing of biomass. By use of a movable, cooled, and quenched gas/particle sampling probe, samples were collected at different positions along the vertical axis in the reactor, corresponding to gas residence times in the range [0.25 – 2.0 s]. The collected particles were subjected to various analyses, including char burnout level, particle size distribution, elemental composition, and particle morphology and composition [Damoe et al., 2017].

The ash formation mechanisms were found to be quite similar, for straw and wood. The degree of conversion (char burnout level) was generally good, at residence times of ≥1 s. The size distribution of the residual fly ash particles, evolved with the residence time. For all ashes at long residence times, a peak of residual ash particles in the range of 20−100 μm was observed. The residual ash particles were rich in Si, K, and Ca. Further, at long residence times, sub-micrometer particles consisting primarily of KCl (condensed aerosols), became abundant in the ashes from straw combustion [Damoe et al., 2017].

[Laxminarayan, 2018] simulated deposit formation in the EFR, in order to investigate the effect of operating conditions and ash chemistry on the rate of deposit formation. Experiments were performed using model biomass fly ash, prepared from mixtures of $K_2Si_4O_9$, KCl, K_2SO_4, CaO, SiO_2 and KOH, as well as three different boiler fly ashes: a wood fly ash, a straw fly ash, and a straw + wood, co-fired fly ash.

The model fly ash particles were mixed with air, and injected into the reactor, to form deposits on an air-cooled probe. The influence of flue gas temperature (589–968 °C), probe surface temperature [300–550 °C], flue gas velocity [0.7–3.5 m/s], fly ash composition, fly ash flux [10000–40000 g/m2/h], fly ash particle size [3.5–90 μm] and probe residence time [< 60 min] were investigated [Laxminarayan, 2018].

The results showed that increasing flue gas temperature and probe surface temperature increased the sticking probability of the fly ash particles/deposit surface, thereby increasing the rate of deposit formation. However, increasing flue gas velocity resulted in a decrease in the deposit formation rate, due to increased particle rebound and blow-off effects. Furthermore, it was observed that the deposit formation rate increased with 1) time, 2) fly ash flux, and, 3) fly ash particle size [Laxminarayan, 2018].

[Wang, 2018] investigated the reaction between gaseous K-species (KOH, K_2CO_3, KCl and K_2SO_4), and different Al-Si based additives (kaolin, mullite and coal fly ash), under well-controlled suspension-fired conditions, in the EFR. The K-capture level of the additives, where CK is the mass of potassium captured by 1 g of additive, while XK is the percentage of fed K captured by additive, were quantified by analyzing the solid products. The impact of different parameters, such as the K-concentration in flue gas [50-1000 ppmv], the molar ratio of K/(Al+Si) in reactants [0.048 – 0.961], the reaction temperature [800-1450 °C], the gas residence time

[0.6–1.9 s], the additive particle size, as well as the type of coal fly ashes on the K-capture reaction, was studied [Wang, 2018].

Thus, a lot of the issues mentioned in the Biofficiency application, was already addressed, when the project was initiated. At an early PC-meeting within Biofficiency, it was therefore decided to focus attention on the effect of additives on deposit formation in PF-fired systems, and use the suite of fuels and additives chosen in Biofficiency for this investigation.

In Task 4.1., DTU has conducted combustion tests of biomasses with and without kaolin or well-characterized coal fly ash (CFA), as additive. This work done is reported in details below, as part 1 of D4.1. The experiments have been conducted mainly by MSc-students Semira Naimi and Jesper Thor Funch, under the supervision of PostDoc Guoliang Wang, and Ass. Profs Peter Arendt Jensen and Flemming Jappe Frandsen, DTU. The work of Semira and Jesper is reported in details in their MSc-Thesis [Naimi and Funch, 2019].

ECN has undertaken similar combustion tests in their Lab-scale Combustion Simulator (LCS). The focus will be on the formation of NOx, using methodology previously validated in EU-RFCS project MINORTOP and several commercial projects. Further, additional work carried out investigating slagging, fouling and submicron particle formation is reported. These data are reported as Part 2 (Chapter Additional work) of D4.1.

Part I:

Performance of Fuels in the DTU Entrained Flow Reactor – Influence of Additives on Deposit Formation

1. Fuels, Additives and Experimental Set-Up

As part of Biofficiency five fuels, and their potential for deposit formation, were investigated. The five fuels were pre-selected to show the diversity in composition, often encountered when utilizing biomass fuels;

- Fuel A: Milled wood pellets
- Fuel B: Steam Exploded (SE) bark
- Fuel C: Hydrothermally carbonized (HTC) leaves -
- Fuel D: Danish wheat straw

Table 1: Proximate and ultimate analysis of fuels A, B, C and D. INA = Information Not Available [Naimi and Funch, 2019].

Parameter:	Fuel A	Fuel B	Fuel C	Fuel D
Proximate analysis				
Moisture [%]	6.7	INA	6.12	10
Volatiles [%]	83.3	INA	60.66	INA
Ash content [%]	1.14	4.6	13.86	5.57
Fixed Carbon [%]	INA	INA	19.35	INA
Ultimate analysis				
C	47.96	52.4	48.54	45.93
H	6.09	5.8	4.79	5.86
N	0.13	0.35	0.83	0.64
S	0.07	0.03	0.09	0
O [calculated]	37.91	36.82	25.77	32
LHV [MJ/kg]	17.16	19.76	18.29	INA

Fuel proximate and ultimate analyses are provided in *Table 1*. Three of the fuels; A, B and C, were delivered by the Technical University of Munich (TUM), whilst the Fuel D was supplied from DTU's own fuel storage, mainly in order to include a fuel with a high content of ash, and – even more importantly – a significant K-content in the ash, since K will soften the ash, and thereby may cause significant deposit formation. Fuel D may be considered as a kind of worst case scenario [Frandsen, 2011].

The ash elemental analysis of each fuel, is shown in *Figure 2*, from which some preliminary observations can be made;

- All fuels have a significant Si- and Ca-content [> 9 % Si and > 22 % Ca], although with the Ca-content of fuel D being lower, than the other three fuels.
- Only fuels A and D have high K-content.
- The low K-content in fuels B and C, indicate that - perhaps - in-sufficient amounts of K-species are present, and that they may therefore only cause a minimum of deposit formation.
- Fuels A, B and C, all have a certain Al-content [~ 1-2 %], which will most likely have a self-induced alkali-capturing effect on K-species released from these fuels.
- Finally, fuels B, C and D have a relative high ash-content, when compared to fuel A, which is important, since a too low ash-content may cause a limited amount of ash deposit.

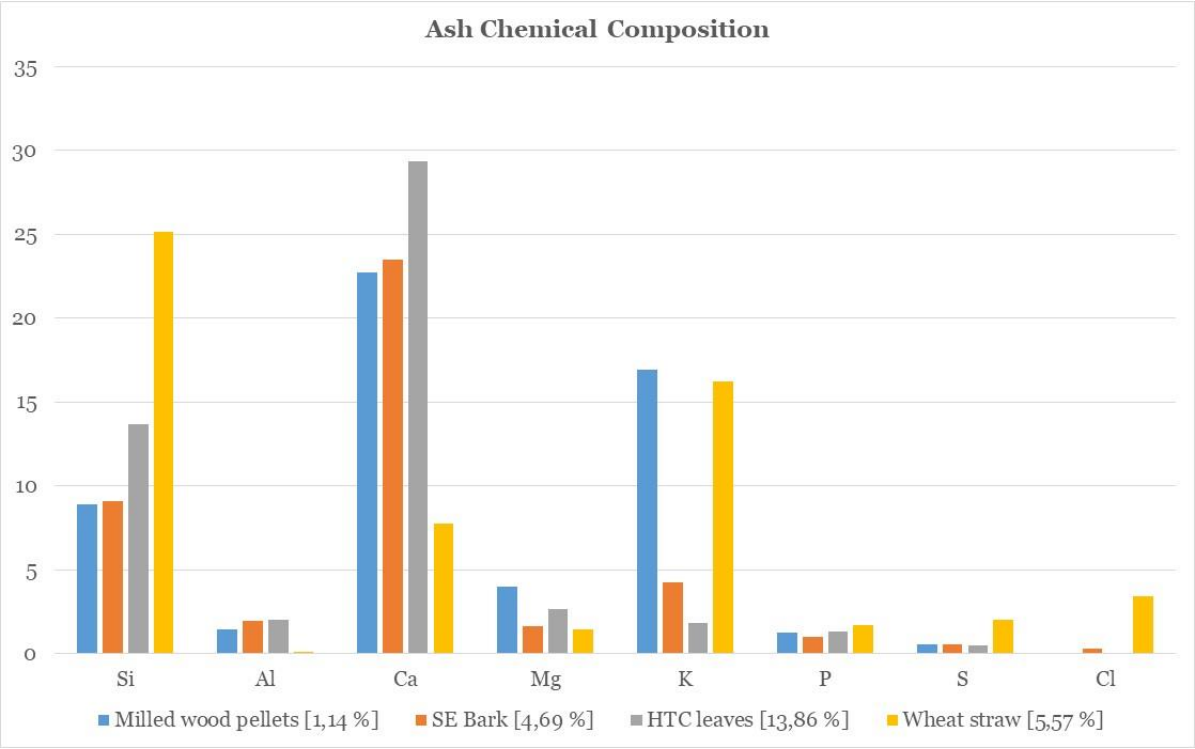

Figure 2: Ash elemental analysis (%wt) of the fuels investigated in this work. The data is based on data from TUM and DTU [Naimi and Funch, 2019].

The additives utilized in the experiments, were [Naimi and Funch, 2019];

- Additive A: Coal fly ash (CFA) from HOFOR - delivered by TUM.
- Additive B: CFA from Asnæs - delivered by Ørsted.
- Additive C: Kaolin - delivered by Technical Research Centre of Finland (VTT).

The ash chemical composition of the three additives, are shown in *Table 2*. Note, that there is a significant difference in the elemental composition between the two CFA additives, A and B. The large amount of residual carbon in additive A could potentially cause additional char oxidation for this additive. However, the amount of additives added must be substantial, in order to have any real impact on the flue gas composition in pilot scale testing. Additionally, the Al_2O_3-content in additive A is lower than in additives B and C, which - initially - could indicate that it would be a less efficient K-capture additive.

The experiments were carried out in an Entrained Flow Reactor (EFR), consisting of a gas supply system, a screw feeder for injecting solids, a gas preheater, a 2 m long electrically heated furnace, and, a fly ash deposition system comprising of an air-cooled deposit probe. A schematic representation of the setup is shown in *Figure 3*.

Table 2: Ash chemical composition of the additives investigated. The data is based on elementary analyses performed by TUM, DTU and VTT. All composition values, are given as %wt [Naimi and Funch, 2019].

Parameter:	CFA HOFOR	CFA Asnæs	Kaolin
SiO_2	51,79	54,39	50
Al_2O_3	22,92	29,7	37,76
CaO	5,96	5,28	0,05
MgO	1,75	1,16	0,35
K_2O	1,78	1,21	2,26
Na_2O	0,8	0,42	0,07
Fe_2O_3	5,85	3,7	0,98
TiO_2	1,08	1,49	0,1
P_2O_5	1,15	1,31	0,1
Residual C	6	0,6	<0,1
d10, microns	3,6	5,1	1,3
d50, microns	22,1	20,6	4,8
d90, microns	83,8	111,9	16,3

After the furnace, the entrained flow entered a bottom chamber, where ash deposits formed on a steel tube (type 316), simulating deposit formation on the first row of platen superheater tubes in boilers. In each experiment, the steel deposit tubes were used as received, without any pre-oxidization. The steel tube, with an outer diameter of 10 mm, a thickness of 1 mm, and a length of 140 mm, was mounted on a retractable annular cooled probe (diameter of 8 mm), as shown in *Figure 4*.

Further details on the DTU EFR are provided by [Damoe et al., 2017; Wang, 2018; Laxminarayan, 2018]

The deposition probe was cooled using air, preheated to 200 °C. Thermocouples were mounted on the outer surface of the deposit probe (and thereby, in contact with the inner surface of the steel tube), and the temperature at the axial centerline of the reactor (referred to as probe surface temperature, see *Figure 4*), was controlled electronically.

The bottom chamber of the EFR was water-cooled, resulting in a decrease in the flue gas temperature. Therefore, the flue gas temperature in the bottom chamber was measured, by replacing the deposit probe with a suction pyrometer. It should be noted that the fly ash particles might not cool down as rapidly as the flue gas, possibly resulting in higher particle temperatures, when compared to the measured flue gas temperature, in the bottom chamber.

The fly ash deposition process was recorded by a high-speed camera, mounted on a port in the bottom chamber (see *Figure 4*). After deposit formation for a specified time duration, the deposit probe was removed, and the deposit was removed and weighed.

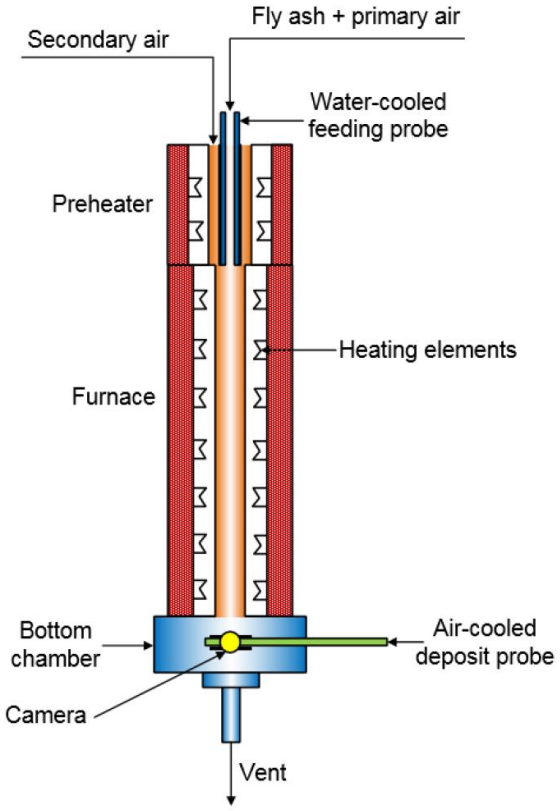

Figure 3: Schematic representation of the Entrained Flow Reactor [Laxminarayan, 2018].

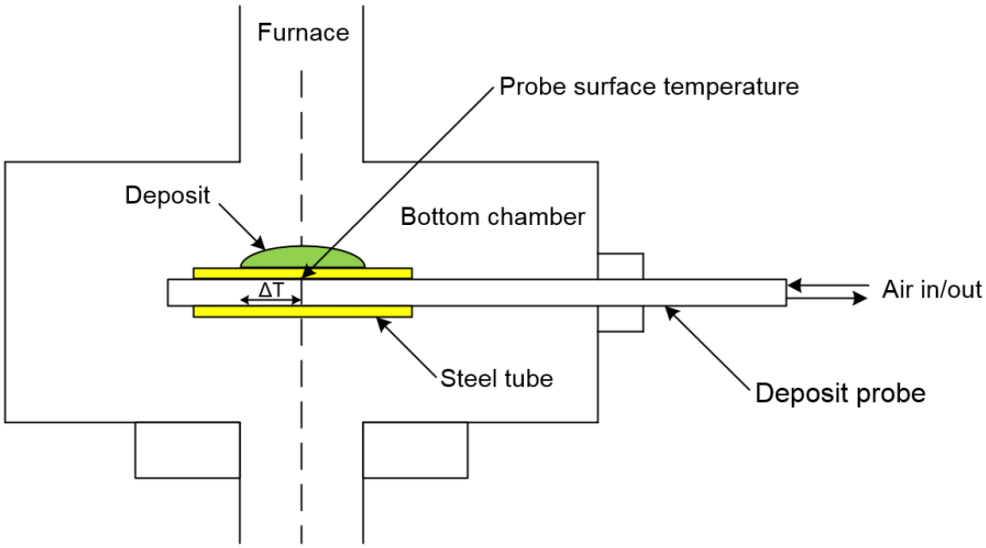

Figure 4: Air-cooled deposit probe. Deposits are formed on the steel tube mounted on the probe [Laxminarayan, 2018].

The reactor temperature was set in the range [1100 – 1350 °C], while the probe temperature was set in the range [500-600 °C].

For a fuel with the main component molar composition $C_\alpha H_\beta S_\gamma N_\delta O_\varphi.(H_2O)_\mu$ the stoichiometric reaction between the fuel and oxygen (O_2) from the combustion air is given as [Naimi and Funch, 2019];

$$C_\alpha H_\beta S_\gamma N_\delta O_\varphi.(H_2O)_\mu + \left(\alpha + \frac{\beta}{4} + \gamma + \frac{\delta}{2} - \frac{\varphi}{2}\right) O_2 \rightarrow$$

$$\alpha\, CO_2 + \left(\frac{\beta}{2} + \mu\right) H_2O + \gamma\, SO_2 + \delta\, NO \qquad (1)$$

Assuming that all N(itrogen) in the fuel, is converted into nitric oxide (NO). The stoichiometric air requirement is then given by:

$$L_{min} = \frac{\alpha + \frac{\beta}{4} + \gamma + \frac{\delta}{2} - \frac{\varphi}{2}}{y_{O2}} \qquad (2)$$

Where y_{O2} is the molar fraction of oxygen in the combustion air. Finally, the air excess number, λ, is defined as:

$$\lambda = \frac{L}{L_{min}} \qquad (3)$$

Knowing λ, the composition of the flue gas can be calculated according to eqn. (1) above. All experiments were conducted at $\lambda \approx 1{,}3$, giving $[O_2] \approx 4{,}6 – 6{,}2$ % [Naimi and Funch, 2019].

The additive dosing rate was calculated, assuming that the K-species in the flue gas reacts one-to-one with the Al and Si, in the given additive to form K-aluminumsilicates. The Si in the additive is assumed to be of limited importance, since it is readily available in both the fuels and additives. The scope of Biofficiency, is to investigate the effect of dosing a relative fixed additive amount, based on the fuels content of K. By neglecting the differences in the elementary compositions of the fuels, and focus only on the problematic element, K, a relative dosing amount can be based on a one-to-one ratio of K in the fuel and Al in the additive, see eqn. (4), where the reference mass of K and Al are obtained from elementary compositions of the fuels, shown in Figure 1 [Wang, 2018],

$$(K/Al)_{ratio} = \frac{(x_{K,fuel}/M_K)\cdot m_{fuel}}{(x_{Al,additive}/M_{Al})\cdot m_{addidive}} \qquad (4)$$

Here $x_{K,fuel}$ and $x_{Al,additive}$ are the fraction of K and Al in the fuel and additive, respectively, m_{fuel} and $m_{additive}$ are the mass of fuel and additive. Finally, M_K and M_{Al} are the molar masses of K and Al, respectively.

The actual deposit mass on the probe is the combined weight of deposit, i.e. up- and downstream, which have build-up during the experiment. The actual total ash captured is the combined weight of the probe deposit, cyclone fly ash sample and aerosol filter sample. The deposit propensity is calculated as the ratio between the measured deposit built-up, and the theoretical estimated build-up, i.e. [Naimi and Funch, 2019];

$$Deposit\ propensity = \frac{m_{Probe\ deposit,measured}}{m_{Probe\ deposit,theoretical}} \qquad (5)$$

The deposit propensity quantifies the extend to which fly ash and aerosols sticks to the surface of probe. The parameter, $m_{Probe\ deposit,\ theoretical}$, is estimated from equation (6).

The theoretical ash deposit is calculated from [Naimi and Funch, 2019]:

$$m_{Probe\ deposit,theoretical} = 90\% \cdot m_{feed} \cdot \frac{A_{probe}}{A_{tube}} \quad (6)$$

Where $m_{Probe\ deposit,\ theoretical}$ is the theoretical ash deposit that build up on the deposition probe, assuming all ash particles that hit the probe would stay on the probe. 90 % is the fraction of ash entrained by flue gas and pass by the deposit probe. The rest of the flue gas (10 %) was pumped to the ventilation directly. m_{feed} is the mass of the ash (including fuel ash and additive) fed into the reactor tube. A_{probe} is the projected area of the deposition probe. A_{tube} is the inner area of the reactor tube.

The ash capture percentage is given by [Naimi and Funch, 2019];

$$Ash\ captured, \% = \left(\frac{m_{ash,actual}}{m_{ash,theoretical} \cdot 0{,}9}\right) \cdot 100\% \quad (7)$$

Where the 0.9 (or 90 %) are multiplied onto the theoretical ash amount, as approximately 10 % of the flue gas is send to gas analyzer, and thus a 10% ash loss is accounted for. The mass% of lost ash is then simplify computed as [Naimi and Funch, 2019];

$$Ash\ lost, \% = 100\ \% - Ash\ captured, \% \quad (8)$$

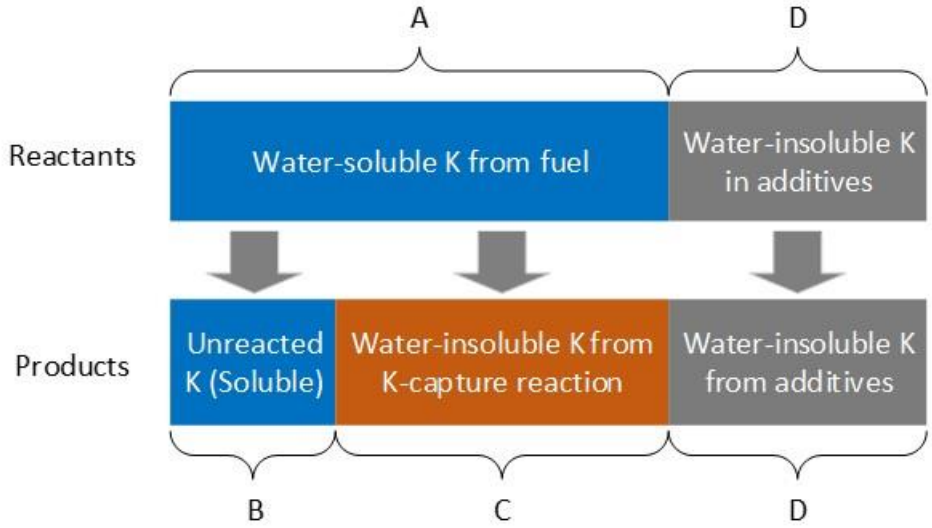

Figure 5: Potassium transformations in the K-capture reaction [Wang, 2018].

Two parameters are used for quantifying the amount of K captured by additives: [1)] the K-conversion (X_K), and [2)] the K-capture level (C_K). X_K is defined as the percentage (%) of input fuel-K, chemically captured by solid additives forming water-insoluble K-aluminosilicate, while C_K is the mass of K captured by 1 g of additive (g K/g additive) [Wang, 2018].

As shown in *Figure 5*, K in the reactants originated both from the fuel and the additives (kaolin or coal fly ash). The majority of K in the reactants was from the fuels, which was water-soluble (part A). The remaining K was from additives and was water-insoluble (part D). During the K-capture, a part of the water-soluble K reacted with additives forming water-insoluble K-aluminosilicate (part C in the products), while the unreacted K-salts remained water-soluble (part B). The K-conversion (X_K), and K-capture level (C_K) were calculated, based on ICP-OES analyses of reacted samples

as shown in Equation (9-10). Detailed information on calculation method is provided by [Wang, 2018].

$$X_K = \frac{C}{A} \cdot 100\% \quad (9)$$

$$C_K = \frac{n_{K-fuel} \cdot M_K \cdot X_K}{m_{ad.}} \quad (10)$$

In Equation (9), C is the amount of water-insoluble K formed by the K-capture reaction, and A is the amount of K from fuels fed into the reactor, as shown in Figure 5. $n_{K\text{-fuel}}$ (mol) is the molar amount of water-soluble K fed into the reactor, M_K is the molar mass of K (39 g/mol) and $m_{ad.}$ is the mass of solid additives fed into the reactor (g).

The ash collected from the up- and downstream side of the probe, the cyclone and on the aerosol filter were analyzed, in order to determine the chemical composition of the ash samples. XRD analysis was performed at the Department of Chemistry, DTU, in order to obtain also information on chemical species in the ash samples.

The following ash samples, were ICP-analyzed at Force Technology [Naimi and Funch, 2019];

- Samples from **milled wood (fuel A1)** experiments:
  - Deposit sample: Si, Al, Cl, K and water-soluble K.
  - Fly ash + Aerosol sample: Si, Al, Cl, K and water-soluble K.
- Samples from **SE bark (fuel B)** experiments:
  - Deposit sample: Si, Al, Cl, K and water-soluble K.
  - Fly ash + Aerosol sample: Si, Al, Cl, K and water-soluble K.
- Samples from **HTC treated leaves (fuel C)** experiments:
  - Deposit sample: Si, Al, Cl, K, water-soluble K, Ca and water-soluble Ca.
  - Fly ash + Aerosol sample: Si, Al, Cl, K, water-soluble K, Ca and water-soluble Ca.
- Samples from **Danish wheat straw (fuel D)** experiments:
  - Deposit sample: Si, Al, Cl, K, water-soluble K, Ca and water-soluble Ca.
  - Fly ash + Aerosol sample: Si, Al, Cl, K, water-soluble K, Ca and water-soluble Ca.

Further, fly ash from the cyclone, and, aerosols from the filter, were analyzed by TGA (Thermo Gravimetric Analysis), in order to determine the burnout.

2. Experimental Plan and Results

All experiments with/without additive dosing are listed in Table 3, while the ash samples collected, are listed in Table 4.

The reason for performing each experiment is in brief;

- **B1**: Make a base case for deposit formation when firing fuel D, that can later be evaluated against additive dosing experiment.
- **B2**: Investigate the influence of kaolin on deposit formation when firing fuel D. Deposit built-up was compared with base case B1.
- **B3**: Investigate the influence of CFA-Asnæs on deposit formation when firing fuel D. Deposit built-up was compared with base case B1.
- **B4**: Investigate the influence of CFA-HOFOR on deposit formation when firing fuel D. Deposit built-up was compared with base case B1.
- **B5**: Investigate the influence of increased additive dosing on the formation of deposit when firing with fuel D. Deposit built-up will be compared base case B1 and additive dosing case B2.
- **B6**: Make a base for deposit formation when firing fuel C.
- **B7**: Make a base for deposit formation when firing fuel B.
- **B8**: Make a base for deposit formation when firing fuel A, that can later be evaluated against additive dosing experiment.
- **B9**: Investigate the influence of Kaolin on deposit formation when firing fuel A. Deposit built-up was compared with base case B8.
- **B10**: Investigate the influence of CFA-Asnæs on deposit formation when firing fuel A. Deposit built-up was compared with base case B8.
- **B11**: Investigate the influence of CFA-HOFOR on deposit formation when firing fuel A. Deposit built-up was compared with base case B8.
- **B12**: Investigate the repeat ability of the experiments by performing experiment B2 again. B2 and B12 can then be compared.

2.1. Experiment B1, Wheat Straw, No Additive

Experiment B1 was conducted with fuel D - wheat straw, which have an ash-content of 5.57%, and a K-content of 16.23 wt% on an ash basis.

Figure 6: Photo of deposit probe upon completion of experiment. Operational data from experiment B1: Fuel = fuel D - wheat straw, fuel feed rate = 469 g/hr, Additives = NA, Furnace Temp. = 1350℃, surface temperature of probe = 600℃, λ= 1.3, residence time = 2 s [Naimi and Funch, 2019].

No additive was utilized in experiment B1. The run time was 40 minutes and Table 4 summarizes the weight of the collected solid samples from the experiment, as well as the ash capture ratio.

Table 3: List of experiments performed. The estimate deposit on probe [g] is calculated assuming all ash flux stick to the probe [Naimi and Funch, 2019].

No.	Fuel	Fuel type	Run time [min]	Additive	Ash content %	Fuel feed rate [g/h]
B1	D	Wheat straw	40	NA	5.57	469
B2	D	Wheat straw	40	Kaolin	8.44	472
B3	D	Wheat straw	40	CFA Asnæs	9.14	507
B4	D	Wheat straw	40	CFA HOFOR	10.20	506
B5	D	Wheat straw	30	Kaolin	11.14	487
B6	C	HTC leaves	20	NA	13.87	454
B7	B	SE Bark	60	NA	4.60	432
B8	A1	Milled WP	180	NA	1.14	473
B9	A1	Milled WP	180	Kaolin	1.80	479
B10	A1	Milled WP	180	CFA Asnæs	1.97	482
B11	A1	Milled WP	180	CFA HOFOR	2.21	485
B12	D	Wheat straw	40	Kaolin	8.44	472

No.	%K in fuel	%Additive of fuel	K/Al-ratio applied	Ash feed during experiment [g]	Ash flux [g/cm^{2}min]	Estimated deposit on probe [g]
B1	16.23	0.00	102.60	15.66	0.0078	2.49
B2	16.23	3.13	1.05	23.92	0.0119	3.81
B3	16.23	3.98	1.10	27.26	0.0136	4.34
B4	16.23	5.15	1.07	30.28	0.0151	4.82
B5	16.23	6.26	0.56	25.16	0.0167	4.00
B6	1.81	0.00	0.61	21.0	0.0209	3.34
B7	4.26	0.00	1.49	17.87	0.0066	3.16
B8	16.91	0.00	8.10	14.56	0.0018	2.57
B9	16.91	0.67	0.94	23.28	0.0029	4.13
B10	16.91	0.85	0.93	25.68	0.0032	4.12
B11	16.91	1.10	0.97	28.97	0.0036	4.56
B12	16.23	3.13	1.05	26.6	0.0132	4.23

An image of the deposit build-up on the probe is shown in Figure 6. Upon removal of the deposit probe it was observed that a distinct white layer had formed on the downstream side of the probe, which is clearly visible in Figure 6. The individual layer chemical composition was not determined. Further, the deposit formed was observed to be quite compact. Only the uppermost layer fell off easily. A middle black layer was encountered, which had to be physically knocked off, and, lastly a bottom, mostly white, layer was encountered. The bottom most layer had to be brushed off with force [Naimi and Funch, 2019].

Table 4: Ash fed during experiment, mass of collected samples and ash capture ratio for experiment B1-B12 [Naimi and Funch, 2019].

No.	Ash fed [g]	Top of probe [g]	Bottom of probe [g]	Cyclone [g]	Aerosol filter [g]	Ash capture:
B1	15.66	1	0.1	4.8	1	0.383
B2	23.00	1	0.1	6.8	1	0.391
B3	27.26	1	0.1	6.6	1	0.315
B4	30.28	0.8	0.1	6.4	0.8	0.268
B5	25	0.776	0.013	8.1	0.9	0.389
B6	18.94	0.3	0.1	2.1	0.7	0.169
B7	19.9	0.351	0.016	2.8	0.518	0.235
B8	16.2	0.229	0.034	1.438	0.762	0.257
B9	23.28	0.507	0.042	3.328	1.085	0.264
B10	25.68	0.77	0.059	4.071	1.15	0.236
B11	28.97	0.846	0.074	6.599	1.297	0.304
B12	27.2	1.0	0.1	4.5	1.1	0.291

2.2. Experiment B2, Wheat Straw, 3.13 wt% Kaolin

Experiment B2 was conducted with fuel D - wheat straw, dosed with kaolin, as additive. The kaolin was dosed in a 3.13 wt% ratio, and pre-mixed with the fuel. The run time was 40 minutes and Table 4 summarizes the weight of the collected solid samples from the experiment as well as the ash capture ratio.

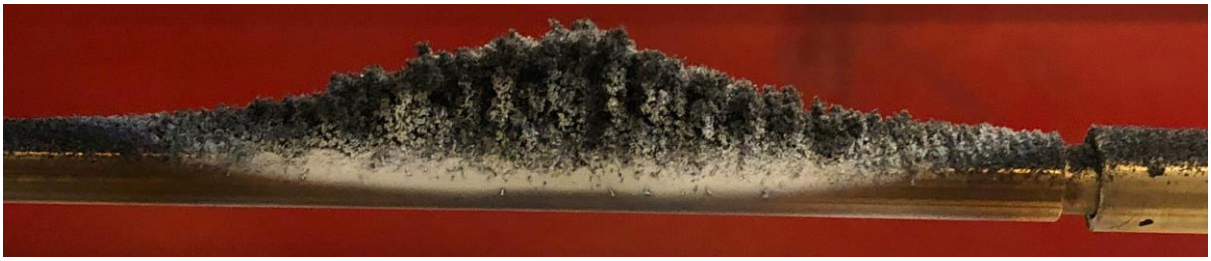

Figure 7: Photo of deposit probe upon completion of experiment. Operational data from experiment B2: Fuel = fuel D - wheat straw, fuel feed rate = 458 g/hr, Additives = Kaolin (Additive C), wt.% additive = 3.13, Furnace Temp. = 1350°C, surface temperature of probe = 600℃, λ = 1.3, residence time = 2 s [Naimi and Funch, 2019].

An image of the deposit build-up on the probe is shown in Figure 7. The deposit had a very porous structure, the outermost layer of the deposit was very loose, and could be removed simply by rotating the probe. Underneath the outer layer was a middle layer, which was more compact, dark in color, and was found to be more sintered. Substantial physical force, had to be applied to the middle layer, in order to remove it. Finally, a white inner layer, was hard, and had to be brushed off with force [Naimi and Funch, 2019].

2.3. Experiment B3, Wheat Straw, 3.98 wt% CFA Asnæs

Experiment B3 was conducted with fuel D - wheat straw, dosed with CFA Asnæs, as additive. The CFA Asnæs was dosed in a 3.98 wt% ratio, and was pre-mixed with the fuel. The run time was 40 minutes and Table 4 summarizes the weight of the collected solid samples from the experiment as well as the ash capture ratio.

Figure 8: Image of deposit probe upon completion of experiment. Operational data from experiment B3: Fuel = fuel D - wheat straw, fuel feed rate = 488 g/hr, Additives = CFA Asnæs (Additive B), wt.% additive = 3.98, Furnace Temp. = 1350°C, surface temperature of probe = 600 °C, λ = 1.3, residence time = 2 s [Naimi and Funch, 2019].

An image of the deposit build-up on the probe is shown in Figure 8. After removal of the deposit probe, it was observed that the upper and outermost deposit layer was very loose in structure, and could easily be removed. Beneath it was almost completely black middle layer, which was more dense and harder to remove, most likely due to stronger sintering. Finally, an inner white layer could only be removed by brushing. In general, the deposit formed was observed to be more dense than the one observed in experiment B2 (fuel D - wheat straw and kaolin), yet it still had a distinct porous appearance [Naimi and Funch, 2019].

2.4. Experiment B4, Wheat Straw, 5.15 wt% CFA HOFOR

Experiment B4 was conducted with fuel D - wheat straw, dosed with CFA HOFOR, as additive. The CFA HOFOR was dosed in a 5.15 wt% ratio, and was pre-mixed with the fuel. The run time was 40 minutes, and Table 4 summarizes the weight of the collected solid samples from the experiment as well as the ash capture ratio.

An image of the deposit build-up on the probe is shown in Figure 9. The outermost layer was found to be very loose (lightly-sintered), and could be removed by simply turning the probe upside down. Underneath the outermost layer a second, mostly black, middle layer had formed. This layer was more compact and required a much stronger force to remove, by e.g. physical knocking the probe against a solid object. At the surface of the probe, a thin white layer had formed. This layer required physical brushing to be removed. In general, the deposit formed, was observed to be alike the deposit from experiment B3, in regards to porosity and overall structure layout, see Figure 8 [Naimi and Funch, 2019].

Figure 9: Image of the deposit probe after experiment B4. Operational data from experiment B4: Fuel = fuel D - wheat straw, fuel feed rate = 482 g/hr, Additives = CFA HOFOR (Additive A), wt.% additive = 5.15, Furnace Temp. = 1350°C, surface temperature of probe = 600℃, λ = 1.3, residence time = 2 s [Naimi and Funch, 2019].

2.5. Experiment B5, Wheat Straw, 6.26 % Kaolin

Experiment B5 was conducted with fuel D - wheat straw, dosed with kaolin as additive.

The kaolin was dosed in a 6.26 wt% ratio, and was pre-mixed with the fuel.

Figure 10: Image of deposit probe upon completion of experiment B5. Operational data from experimentB5: Fuel = fuel D - wheat straw, fuel feed rate = 489 g/hr, Additives = Kaolin (Additive C), wt.% additive = 6.26, Furnace Temp. = 1350°C, surface temperature of probe = 600 ℃, λ = 1.3, residence time = 2 s [Naimi and Funch, 2019].

It was in previous experiments discovered that with increased additive dosage, the probe deposit built-up was very loose. To ensure the entire probe deposit could be extracted, WD40 grease was applied to the probe removal routine, in order to ensure a smooth, non-bumpy removal of the probe from the bottom chamber. Additionally, the experiment was only run for 30 minutes, as the deposit built-up was very fast and extensive. Otherwise, the exact same procedure and operating conditions as in experiment B5E, was applied. The dosing of additive (6,26 wt.%) kaolin, lead to a low K/Al ratio of 0,5 compared to the K/Al molar ratio of 1, used in experiments B2, B3 and B4. Table 4 summarizes the weight of the collected solid samples from the experiment as well as the ash capture ratio [Naimi and Funch, 2019].

An image of the deposit build-up on the probe is shown in Figure 10. Upon removal of the deposit probe no sharp, well-defined white layer was visible, in contrast to the three previous fuel D - wheat straw/additive experiments. The layer was now observed to be more grayish in color, and only few white spots could be seen on the outermost layer formed. This visually indicated that the double dosage of additive, had a noticeable effect on deposit formation. In addition, the deposit was very loose. The entire deposit, except for the innermost layer, could be removed simply by turning the deposit probe, upside down. The innermost layer still required brushing to be removed, but there was significant less material to remove [Naimi and Funch, 2019].

2.6. Experiment B6, HTC Leaves, No Additive

Experiment B6 was was done with fuel C - HTC leaves, with an ash content of 13.87 wt%, and a K-content, on an ash basis, of 1.81 wt%. In this experiment no fuel accumulation was observed on the fuel conveyor, and the experiment was run for only 20 minutes, due to the high ash-content of fuel C - HTC leaves. Table 4 summarizes the weight of the collected solid samples from the experiment as well as the ash capture ratio [Naimi and Funch, 2019].

Only a very limited amount of deposit was observed on the probe, see Figure 11, consisting of an inner brown/beige layer, which was sticky, but to a less extend than observed in experiment B1-B5, and required physical brushing to remove. On top of the inner layer, a small, very loose, deposit had formed. This layer could be removed by simply turning the probe upside down.

The amount of deposit clearly indicated that this fuel would be non-problematic, in regards deposit built-up on heat exchanger surfaces [Naimi and Funch, 2019].

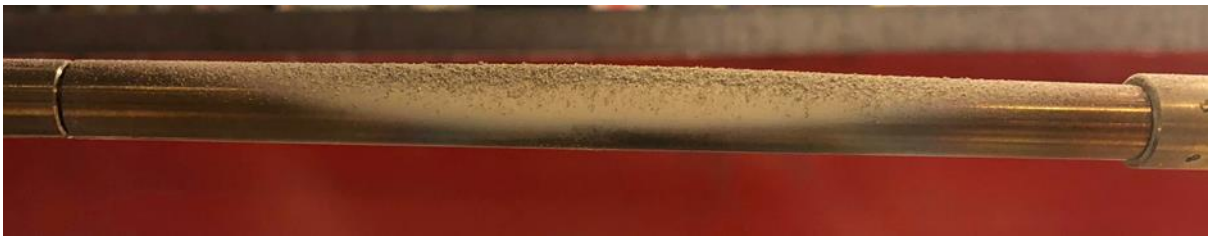

Figure 11: Photos of deposit probe upon completion of experiment. Operational data from experiment B6: Fuel = fuel C - HTC leaves, fuel feed rate = 454 g/hr, Additives = NA, wt.% additive = NA, Furnace Temp. = 1350℃, surface temperature of probe = 600 ℃, λ = 1.3, residence time = 2 s [Naimi and Funch, 2019].

2.7. Experiment B7, SE Bark, No Additive

Experiment B7 was conducted with fuel B - SE bark, and no additive. Fuel B - SE bark had an ash content of 4.60 wt%, and a K-content of 4.26 wt% on an ash basis. The run time was 60 minutes, and Table 4 summarizes the weight of the collected solid samples from the experiment as well as the ash capture ratio.

Upon removal of the probe, it turned out that, only a limited amount of deposit had formed. A thin outer layer of black deposit, had formed on the upstream side of the deposit. This deposit was very loose, and of a salt-grain like structure. The outer layer of deposit was easily removed, by turning the probe upside down. At the surface of the deposit probe, a thin brown layer had formed. This layer had to be removed with brushing. As with the fuel C - HTC leaves experiment, B6, the amount of deposit indicated that the fuel would be non-problematic, concerning deposit built-up on heat exchanger surfaces [Naimi and Funch, 2019].

Figure 12: Photos of deposit probe upon completion of experiment. Operational data from experiment B7: Fuel = fuel B - SE bark, fuel feed rate = 432 g/hr, Additives = NA, wt.% additive = NA, Furnace Temp. = 1350℃, surface temperature of probe = 600 ℃, λ = 1.3, residence time = 2 s [Naimi and Funch, 2019].

2.8. Experiment B8, Milled Wood Pellets, No Additive

Experiment B8 was conducted with fuel A - milled wood pellets, and no additive. The fuel had an ash-content of 1.14 wt.% and a K-content of 16.91 wt% on an ash basis.

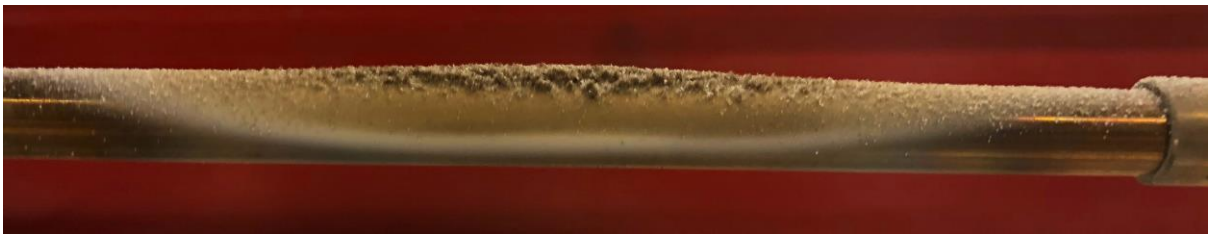

Figure 13: Photos of deposit probe upon completion of experiment. Operational data from experiment B8: Fuel = fuel A1 - milled wood pellet, fuel feed rate = 478 g/hr, Additives = NA, wt.% additive = NA, Furnace Temp. = 1350°C, surface temperature of probe = 600 °C, λ = 1.3, residence time = 2 s [Naimi and Funch, 2019].

The run time was 180 minutes, and Table 4 summarizes the weight of the collected solid samples from the experiment as well as the ash capture ratio. The fuel A - milled wood pellet experiment, were all run for 180 minutes, due to the low ash-content of the fuel.

Upon removal of the deposit probe, three distinct deposits layers were observed [Naimi and Funch, 2019];

- A deposit was formed on the upstream side of the deposit probe, though the amount of deposit was only small. This deposit could be removed by knocking the probe on a solid object, and thereby shaking off the deposit.
- In between the outermost deposit build-up and the innermost layer, a beige-colored layer was formed. This layer was more solid, and had to be removed by brushing.
- Finally, underneath the middle beige layer, a thin white inner layer had formed. Like the middle layer, this innermost layer had to be brushed off with strong force, as it was found to be quite sintered.

2.9. Experiment B9, Milled Wood Pellets, 0.67 wt% Kaolin

Experiment B9 was conducted with fuel A - milled wood pellet, dosed with kaolin as additive. The Kaolin was dosed in a 0.67 wt% ratio, and pre-mixed with the fuel.

Figure 14: Image of deposit probe upon completion of experiment. Operational data from experiment B9: Fuel = fuel A1 - milled wood pellet, fuel feed rate = 476 g/hr, Additives = Kaolin (Additive A), wt.% additive = 0.67, Furnace Temp. = 1350°C, surface temperature of probe = 600℃, λ = 1.3, residence time = 2 s [Naimi and Funch, 2019].

The experiment was similar to experiment B2, just the fuel type and weight of dosed additive was changed, as the K/Al ratio was to be kept at 1. The run time was 180 minutes and Table 4 summarizes the weight of the collected solid samples from the experiment as well as the ash capture ratio [Naimi and Funch, 2019].

A distinct white layer was observed, both as an inner layer, and in spots on the formed deposit built-up, see Figure 14. This observation was surprising, as a less distinct white layer had formed when firing wood pellets without additives. Additionally, the beige layer, observed in

experiment B8, had now completely disappeared, indicating a change in the deposit formation process due to the presence of an additive. The deposit was, however, found to be less sintered than the built-up observed in experiment B8, i.e. when firing fuel A - milled wood pellet without additives [Naimi and Funch, 2019].

2.10. Experiment B10, Milled Wood Pellets, 0.85 wt% CFA Asnæs

Asnæs as additive, in a 0.85 wt% ratio, pre-mixed with fuel. The experiment was similar to experiment B3, only the fuel type and dose of additive was changed, as the K/Al ratio was to be kept equal to 1. The run time was 180 minutes and Table 4 summarizes the weight of the collected solid samples from the experiment as well as the ash capture ratio [Naimi and Funch, 2019].

The same distinct white layer, as observed in experiment B9, was again observed in experiment B10. The observations were much like those for experiment B9, the only major difference being that a larger more pronounced deposit build-up was observed, probably due to the increased additive mass being added. The strength of the different deposit layers, was similar as those done for experiment B9 [Naimi and Funch, 2019].

Figure 15: Photos of deposit probe upon completion of experiment. Operational data from experiment B10: Fuel = fuel A1 - milled wood pellet, fuel feed rate = 478 g/hr, Additives = CFA Asnæs (Additive B), wt.% additive = 0.85, Furnace Temp. = 1350°C, surface temperature of probe = 600℃, λ = 1.3, residence time = 2 s [Naimi and Funch, 2019].

2.11. Experiment B11, Milled Wood Pellets, 1.10 wt% CFA HOFOR

Experiment B11 was also conducted with fuel A - milled wood pellets, dosed with CFA HOFOR dosed in a 1.10 wt% ratio, pre-mixed with the fuel. The experiment was similar to experiment B4, only the fuel type and dose of additive was changed, as the K/Al ratio was to be kept equal to 1. The run time was 180 minutes and Table 4summarizes the weight of the collected solid samples from the experiment as well as the ash capture ratio [Naimi and Funch, 2019].

Figure 16: Photos of deposit probe upon completion of experiment. Operational data from experiment B11: Fuel = fuel A1 - milled wood pellet, fuel feed rate = 480 g/hr, Additives = CFA HOFOR (Additive C), wt% additive = 1.10, Furnace Temp. = 1350°C,surface temperature of probe = 600 ℃, λ = 1,3, residence time = 2 s [Naimi and Funch, 2019].

A distinct white layer, was observed on the deposit probe, much like what was observed in experiments B9 and B10, i.e. the same distinct layer built-up and strength of the layers. Only difference being that a larger deposit built-up was observed, which was again attributed to the fact that a larger mass of additive is added per gram fuel [Naimi and Funch, 2019].

2.12. Experiment B12, Wheat Straw, 3.13 wt% Kaolin

Experiment B12 was conducted in order to serve as a repetitive data validating experiment, and it was therefore natural to compare the deposit built-up to experiment, B2. Table 4 summarizes the weight of the collected solid samples from the experiment as well as the ash capture ratio of experiment B12.

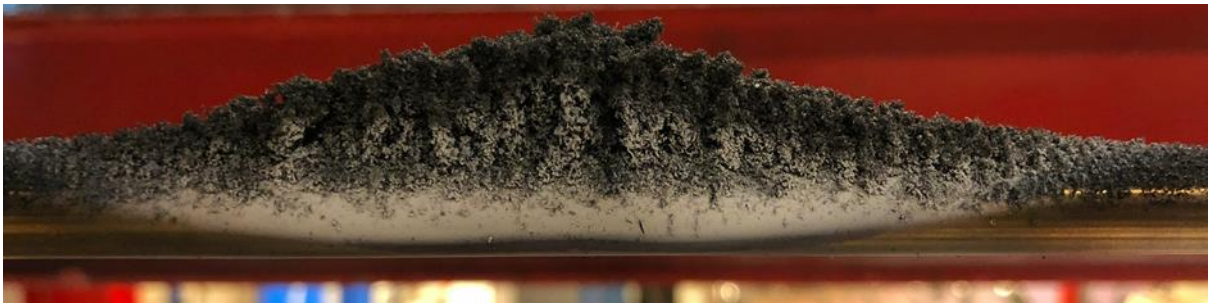

Figure 17: Photos of deposit probe upon completion of experiment. Operational data from experiment B12: Fuel = fuel D - wheat straw, fuel feed rate = 474 g/hr, Additives = Kaolin (Additive A), wt% additive = 3.13, Furnace Temp. = 1350°C, surface temperature of probe = 600 °C, λ = 1,3, residence time = 2 s [Naimi and Funch, 2019].

Layer-wise the same thin white layer was observed, with the additional formation of white spots on the outermost layer of the formed deposit. The deposit, generated in experiment B12, was visually observed to be porous and found to be non-sticky, similar to the deposit from experiment B2 [Naimi and Funch, 2019].

Comparing Figures 16 and 6, the results observed for experiments B2 and B12, were found to be much alike. However, it is noticeable that much less ash was captured in the cyclone, for experiment B12, compared to experiment B2, see Table 4 [Naimi and Funch, 2019].

3. Data Analysis

This chapter contain an outline of the analysis of data conducted.

3.1. TGA Analysis

It was tested, by TGA-analysis, whether complete combustion of the fuels was obtained. The applied TGA procedure heated the collected ash samples up to 700°C, in a N2-atmosphere, in order to devolatilize any non-combustible residues, and, completely dry the collected samples. Then the temperature was lowered to 550 °C, and the atmosphere was switched to O2. The samples were kept at the pyrolysis temperatures for 120 minutes, after which the temperature was gradually increased toward 1300°C, in order to oxidize any leftover chars. The TGA results are summarized below [Naimi and Funch, 2019].

The fly ash samples from experiment B1, was double validated.

- **Fuel D – Danish wheat straw - Experiment B1:**
  (Trail 1) Pyrolysis: 1.948 % mass loss.
  (Trail 2) Pyrolysis: 2.016 % mass loss.
  (Trail 1) Char oxidation: 1.291 % mass loss.
  (Trail 2) Char oxidation: 1.113 % mass loss.
- **Fuel C – HTC Leaves - Experiment B6:**
  Pyrolysis: 2.096 % mass loss.
  Char oxidation: 0.394 % mass loss.
- **Fuel B – SE Bark - Experiment B7:**
  Pyrolysis: 1.067 % mass loss. Char oxidation: 0.501 % mass loss.
- **Fuel A1 – Milled Wood Pellets - Experiment B8:**
  Pyrolysis: 3.906 % mass loss.
  Char oxidation: 0.578 % mass loss.

The TGA data for fly ash samples from fuels D, C and B, all show minor mass losses, i.e. reasonable complete combustion of these fuels were achieved, in good agreement with previous observations by [Damø et al., 2017].

3.2. Repetition of Experiments (Experiment B2 vs. B12)

To verify the repeatability of the experimental data. The deposit propensity (eqn. (5)) obtained for the two experiments B2 and B12, were found to be identical ~ 0.29, indicating that deposit build-up repeatability is possible in the EFR. However, this parameter only relates to the mass of deposit build-up, and not the composition.

The fraction of H_2O-soluble K in deposit respectively fly ash, are shown in Table 5, together with the fraction of aerosols in the fly ash, and the K-conversion and K-capture. A comparison of the chemical compositions of the raw fuel D, deposits and fly ashes is shown in Figure 18, based on ICP-AES data [Naimi and Funch, 2019].

Table 5: Fraction of H_2O-soluble K detected in deposit and fly ash, fraction of aerosols of the total fly ash, and X-conversion and K-capture for experiments B2 and B12 [Naimi and Funch, 2019].

Table 5: Fraction of H_2O-soluble K detected in deposit and fly ash, fraction of aerosols of the total fly ash, and X-conversion and K-capture for experiments B2 and B12 [Naimi and Funch, 2019].

Wheat straw	H_2O-sol K Deposit (%)	H_2O-sol K Fly ash (%)	% Aerosols	K-Conversion, X_K	K-Capture, C_K (g/g)
Fuel D – 3.13 wt% Kaolin (B2)	37	29	13	70	0.28
Fuel D – 3.13 wt% Kaolin (B12)	37	36	20	63	0.26

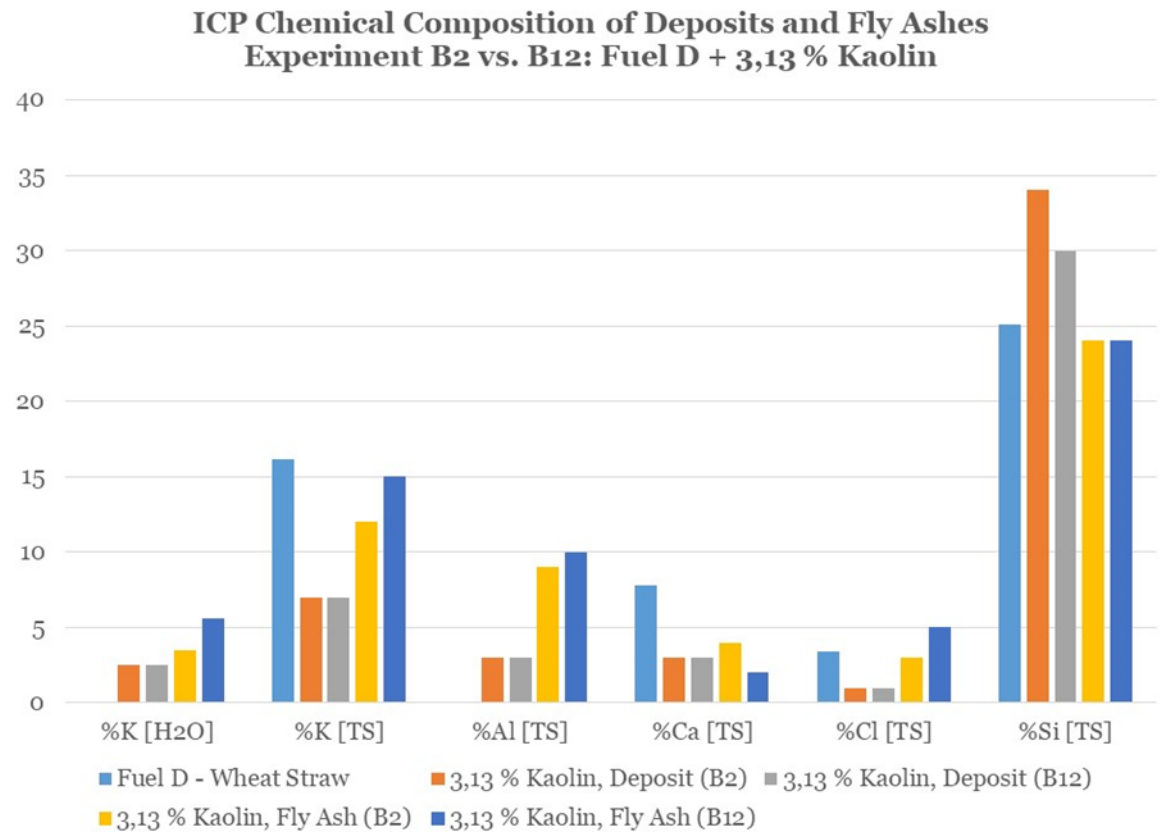

Figure 18: ICP chemical analyses of deposits and fly ashes from experiment B2 and B12.

In Table 5, it is seen that deposits formed in exp. B2 respectively B12, contain the same fraction of H_2O-soluble K (~ 37 %). Anyhow, a significant discrepancy was detected in the fly ash samples, where a higher fraction of H_2O-soluble K, was observed in the B12 fly ash compared to the B2 fly ash. At the same time, more aerosols are formed in B12 compared to B2. This indicate a more efficient release of K from the fuel in B12 compared to B2.

The K-conversion (XK) also reflects a less efficient transformation of H_2O-soluble K to K-aluminumsilicates in B12, compared to B2, while the K-capture (CK) was found to be similar in the two experiments [Naimi and Funch, 2019].

Figure 18 shows ICP-AES elemental analyses of deposits and fly ashes from experiments B2 and B12. The deposits have very similar compositions, while there are small differences between the two fly ashes, with B12 fly ash containing higher levels of both K and Cl, while B2 fly ash had a higher content of Ca.

3.3. Influence of Fuel Type

The deposit propensities for experiments B1, B6, B7 and B8, are shown in Figure 19, while ICP-AES data on the fraction of H_2O-soluble K in the deposits and fly ashes formed, are shown in Table 6, together with the fraction of aerosols detected and the K-conversion estimated in these experiments. Finally, a more detailed chemical composition of the fly ashes and deposits, are shown in Figures 20-21.

Table 6: Fraction of H_2O-soluble K detected in deposit and fly ash, fraction of aerosols of the total fly ash, and K-conversion and K-capture for experiments B1, B6, B7 and B8. NR: Not relevant.

Fuel fed	**H_2O-sol K Deposit (%)**	**H_2O-sol K Fly ash (%)**	**% Aerosols**	**K-Conversion X_K**	**K-Capture C_K (g/g)**
Fuel D Straw (B1)	48	69	17	31	NR
Fuel C HTC Leaves (B6)	21	31	25	70	NR
Fuel B SE Bark (B7)	30	74	15	27	NR
Fuel A Milled WP (B8)	55	86	36	16	NR

Table 6 show that H_2O-soluble K-species in fuel C – SE Bark - undergo a 70% conversion, which is a rather high conversion, indicating that the composition of fuel C (i.e. low K-content and high Al-content) causes K-species to be present in fly ash and deposits as H_2O-insoluble, and thereby less problematic K-Al-Si species. The conversion of H_2O-soluble species to H2O-insoluble species in fuels D, B and A are lower [16-31 %], with fuel A – Milled Wood Pellets - showing only 16% conversion. The conversion of K-species seemingly follows the K/(Al+Si) ratios, i.e. as this ratio increases, a decrease in conversion is observed [Naimi and Funch, 2019].

Fuel A – milled wood pellets – produces the highest fraction of aerosols, most probably due to the low content of ash in this fuel, which allows high concentration of gaseous K-species, and thereby aerosols, to form.

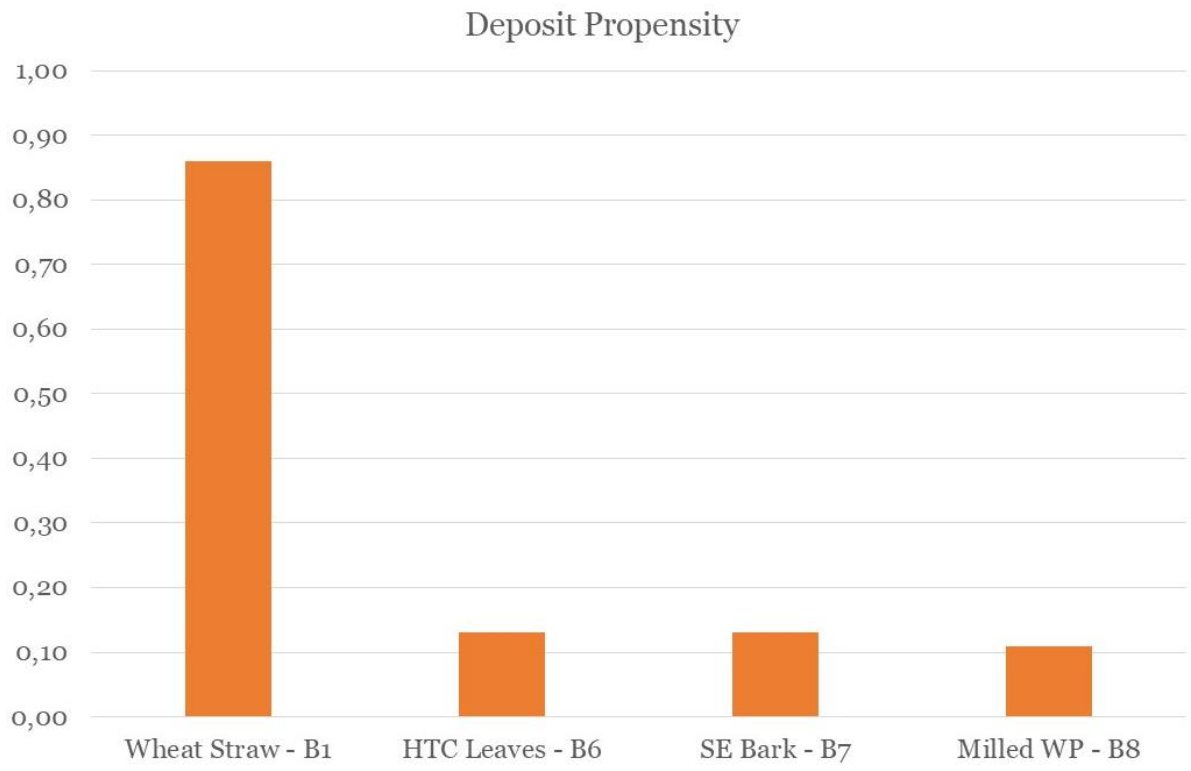

Figure 19: Deposit propensities for experiment B1, B6, B7 and B8. [Figure 36].

In Figure 19, it is seen that Fuel D – Wheat Straw – not surprisingly – is by far the worst fuel, from a deposit propensity point-of-view. When utilizing wheat straw for power production in suspension-fired boilers, one has to apply an additive, to avoid serious deposit formation [Frandsen, 2011]. The other three fuels, show only low deposit propensities, when utilized without an additive. These fuels may actually be utilized without additives.

Figure 20 show the ICP-AES based chemical composition of fly ash and aerosols. It is seen that fuel D – Wheat Straw has the highest concentration of K, Cl and Si in the fly ash+ aerosols. Fuel A – Milled Wood Pellets – also have a relatively high concentration of K in the fly ash. Fuels B and D – HTC Leaves respectively SE Bark – has [as expected] high levels of Ca in the fly ash.

The fly ash chemical composition is reflected in the deposit chemical composition from the different fuels, especially concerning [K], [Ca] and [Si], which are almost mirror images of the fly ash composition. The content of Cl in the deposits is rather low, but here care must be taken, since up- and downstream deposits are blended before ICP-analyses.

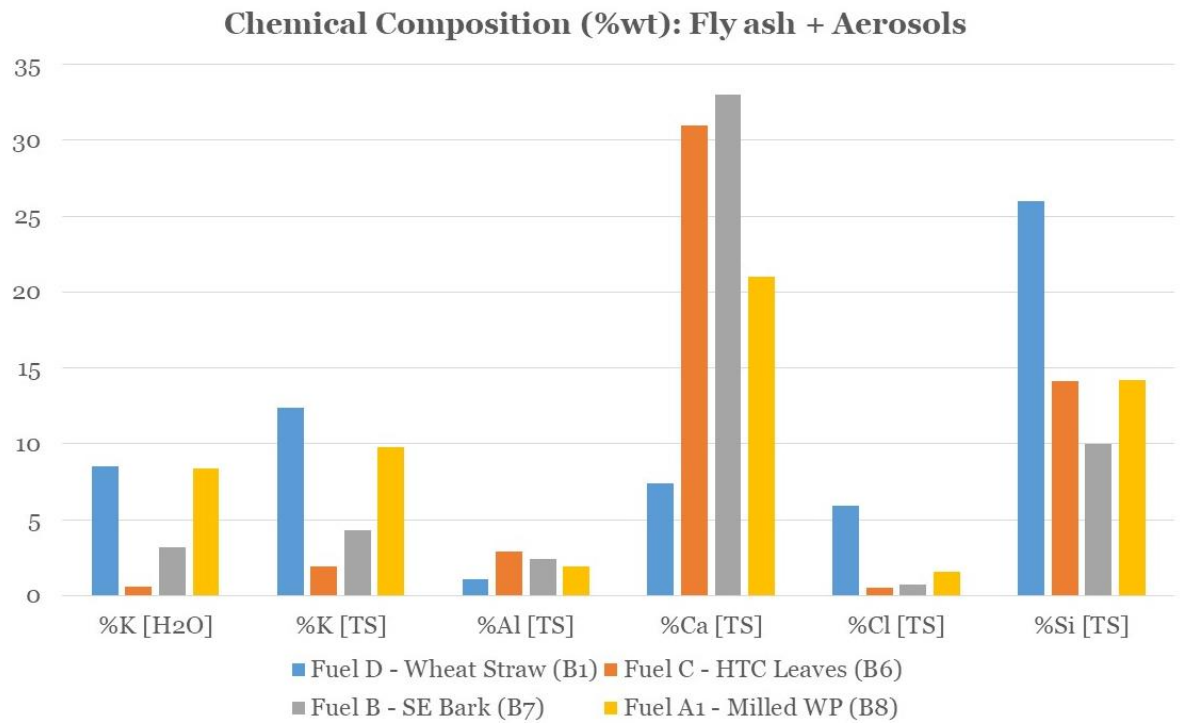

Figure 20: ICP-AES data on fly ash + aerosol chemical composition, experiments B1, B6, B7 and B8.

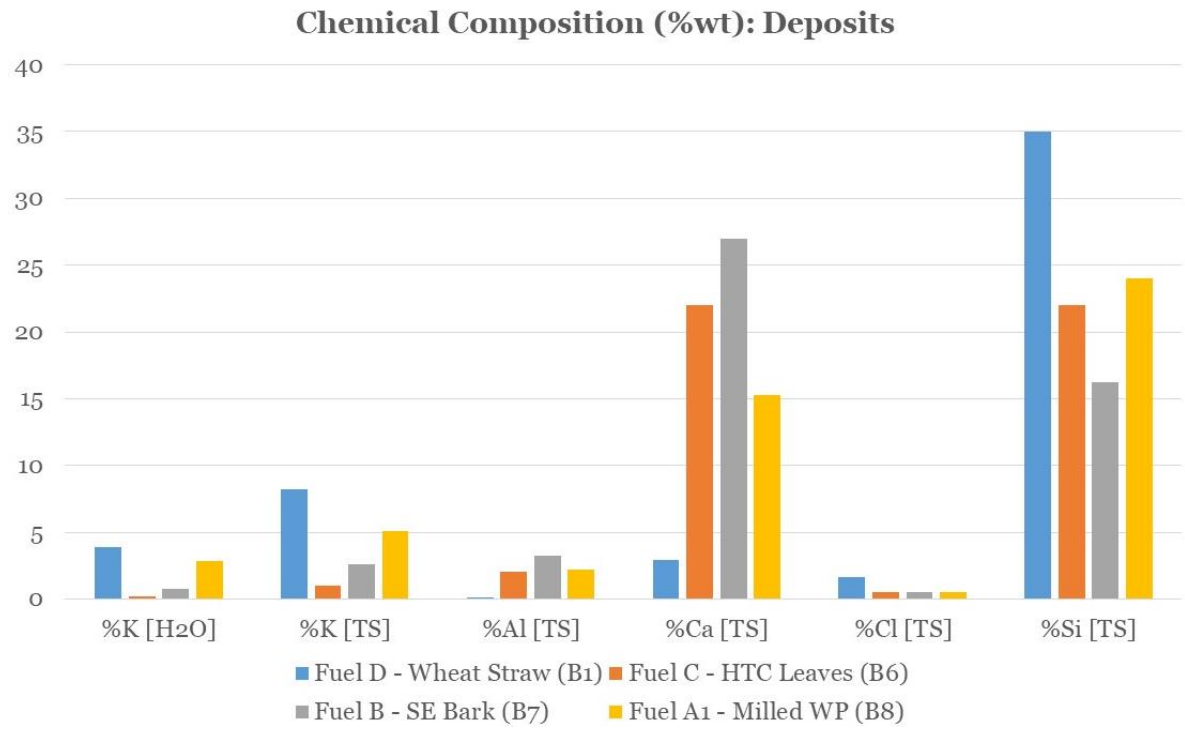

Figure 21: ICP-AES data on deposit chemical composition, experiments B1, B6, B7 and B8.

Usually the amount of downstream deposit is very low, so in reality there may actually be a high [Cl] in some of the downstream deposits, which are then diluted by blending with a factor 10-40 by a high mass of upstream deposit, lean in Cl. Another point is that even Cl in low concentrations, may cause corrosive attack [Naimi and Funch, 2019].

3.4. Influence of Additive Type

The effect of additive type on deposit and fly ash properties, was also investigated. The deposit propensities for experiments B1-B5 (Wheat Straw with additive) respectively B8-B11 (Milled Wood pellets (WPs) with additive), are shown in Figures 22 and 23.

A very clear effect on the deposit propensity is seen in Figure 22, as the deposit propensity decreases from > 0.8 to ≤ 0.2, when additives are dosed to fuel D (Wheat Straw). Thus, fixation of K by the additive causes a significant reduction in deposit formation, which may again affect soot-blowing schedules and cycles in the plant.

In the case of additive-use with fuel A - milled wood Pellets, the additive causes an increase in the amount of deposit formed, and, thereby, also in the deposit propensity, see Figure 23. This effect may be attributed to the fact that the total ash fed to the system is increased when dosing the additives, and the increase in deposit propensity may simply be a result of that.

ICP-AES data on the fraction of H_2O-soluble K in deposits respectively fly ash are shown together with the observed aerosol fraction of the fly ash, and K-conversion as well as K-capture, in Tables 7 and 8.

In Table 7, it can be seen that additive dosing have clear impact on the fraction of H_2O-soluble K, in both the deposit [48 % → 37 %] and fly ash [69 % → <46 %], i.e. the amount of H_2O-soluble, and, thereby, highly mobile K in both deposits and fly ash decreases, when additives are applied.

Table 7: Fraction of H_2O-soluble K detected in deposit and fly ash, fraction of aerosols of the total fly ash, and K-conversion (XK) and K-capture (CK) for experiments B1-B4 [Naimi and Funch, 2019].

Fuel fed	**H_2O-sol K Deposit (%)**	**H_2O-sol K Fly ash (%)**	**% Aerosols**	**K-Conversion, X_K**	**K-Capture, C_K (g/g)**
Fuel D (B1)	48	69	17	31	NR
Fuel D + 3.13 %wt Kaolin (B2)	37	29	13	70	0,28
Fuel D + 3.98 wt% CFA Asnæs (B3)	37	46	13	54	0,20
Fuel D + 5.15 wt% CFA HOFOR (B4)	37	36	10	63	0,20

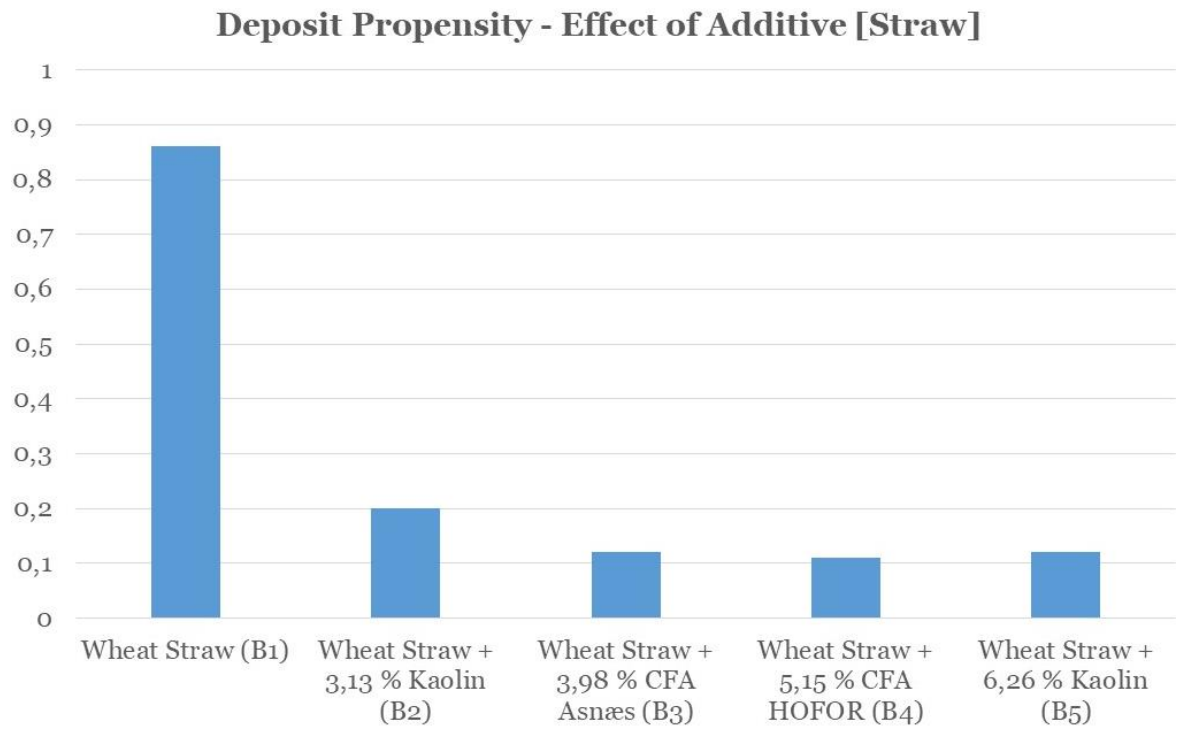

Figure 22: Deposit propensities for experiments B1-B5.

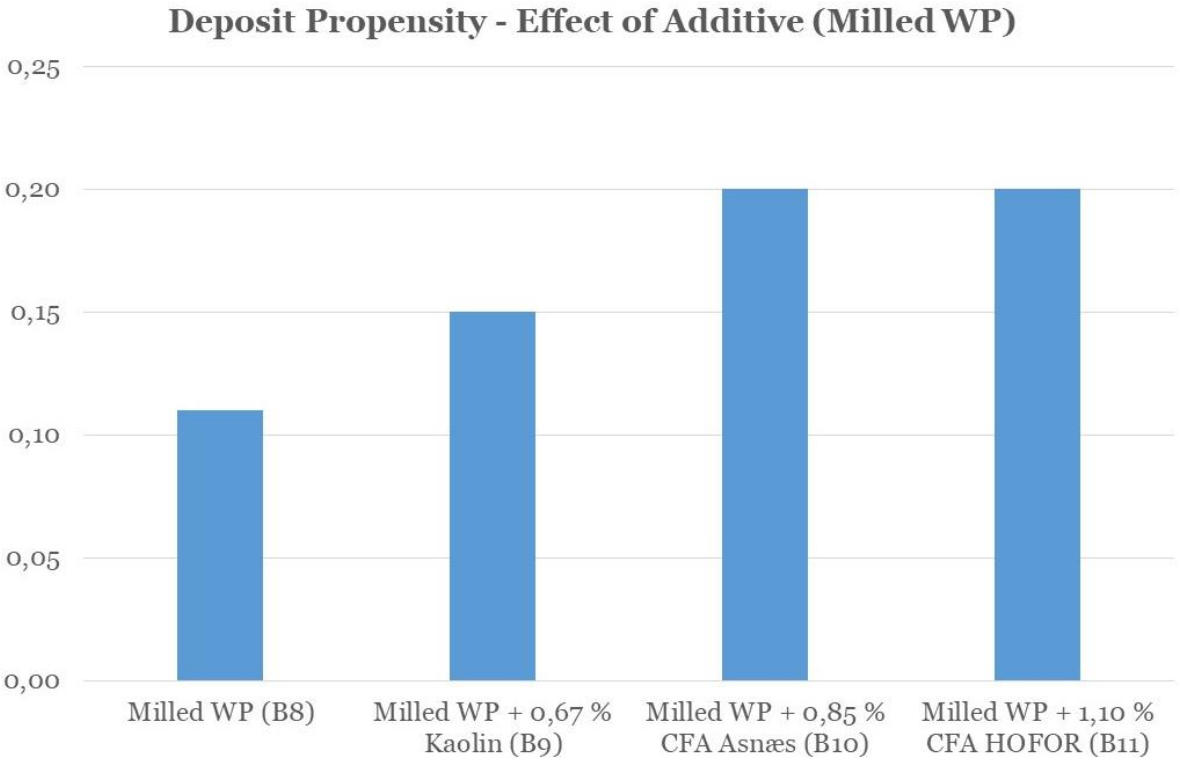

Figure 23: Deposit propensities for experiments B8-B11.

Further, the fraction of aerosols formed decreases [17 % → 13 %], and here seems to be a tendency toward a reverse dependence between the amount additive applied and the fraction of aerosols formed, i.e. more additive means less aerosols. All three additives show high K-conversion [< 54 %], while kaolin have the highest K-capture of the three additives [0,28].

Table 8: Fraction of H_2O-soluble K detected in deposit and fly ash, fraction of aerosols of the total fly ash, and K-conversion (XK) and K-capture (CK) for experiments B8-B11 [Naimi and Funch, 2019].

Fuel fed	H_2O-sol K Deposit (%)	H_2O-sol K Fly ash (%)	% Aerosols	K-Conversion, X_K	K-Capture, C_K (g/g)
Fuel A1 (B8)	55	86	36	16	NR
Fuel A1 + 0,67 %wt Kaolin (B9)	39	42	25	58	0,24
Fuel A1 + 0,85 wt% CFA Asnæs (B10)	31	50	22	51	0,18
Fuel A1 + 1,10 wt% CFA HOFOR (B11)	28	34	16	66	0,18

In Table 8, it can similarly be seen that additive dosing have observable impact on the fraction of H_2O-soluble K, in both the deposit [55 % → < 39 %] and fly ash [86 % → < 50 %]. The amount of H_2O-soluble, and, thereby, highly mobile K in both deposits and fly ash decreases, when additives are applied. Also, the fraction of aerosols formed decreases [36 % → < 25 %], and again it seems to be a tendency toward a reverse dependence between the amount additive applied and the fraction of aerosols formed. All three additives show high K-conversion (X_K) [< 51 %], while kaolin have the highest K-capture (C_K) [0,24] of the three additives.

Thus, both low- and high-K fuels show the same trends in transforming H_2O-soluble K by use of additives. All three additives, i.e. Kaolin and two coal fly ashes show high X-conversion, while Kaolin seems to have the highest K-capture of the three.

A detailed chemical composition of the deposits and fly ashes from experiments B1-B4, fuel D – wheat straw with additive, respectively B8-B11, fuel A - milled wood pellets with additive, are shown in Figures 24-27.

Figures 24-25 shows the chemical composition of deposits and fly ashes, when firing fuel D – Wheat Straw - with additives. For the deposits, it is obvious that additives have an effect on H_2O-soluble [K], total [K], [Cl] and [Si] [all decreasing], and, [Al] [increasing].

For the fly ash composition it can be seen in Figure 25, that kaolin possess the largest reduction effect on both H_2O-soluble [K] and [Cl], as a reduction of 5 % H2O soluble [K] and 3,3 % Cl, is observed. In contrast, CFA Asnæs and CFA HOFOR reduces H_2O-soluble [K] by 3.3 % respectively 4.6 %; and Cl by 2.2 % respectively 2.7 %. This is attributed to the finer particle size of the kaolin additive, which reduces the diffusion limitation for K, into the pores of additive particles.

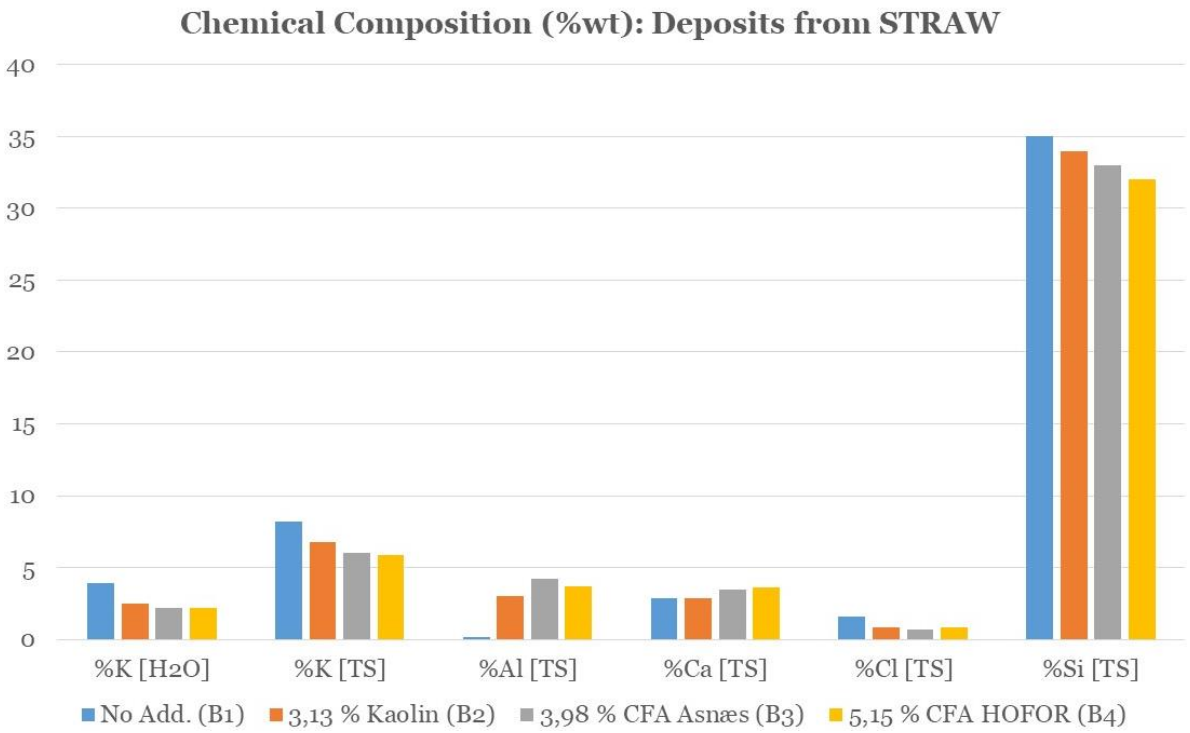

Figure 24: Chemical composition (based on ICP-AES) of deposits formed while firing wheat straw (fuel D) with additives, in experiments B1-B4. [Figure 39].

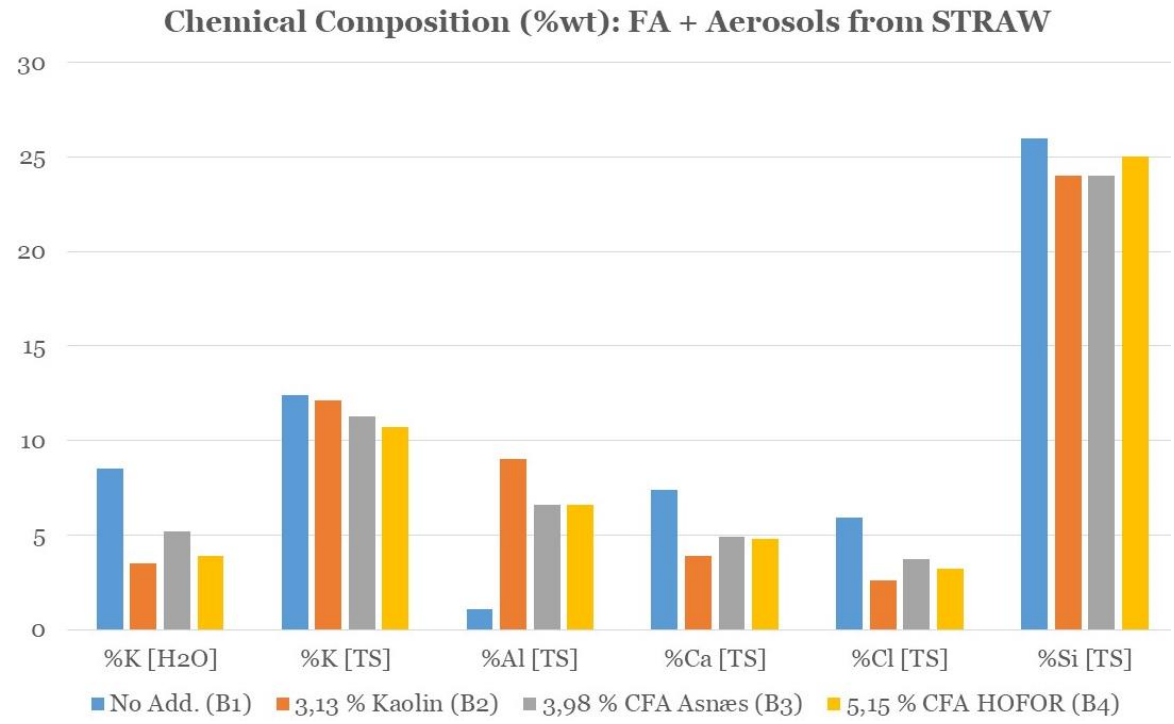

Figure 25: Chemical composition (based on ICP-AES) of fly ash+ aerosols formed while firing wheat straw (fuel D) with additives, in experiments B1-B4.

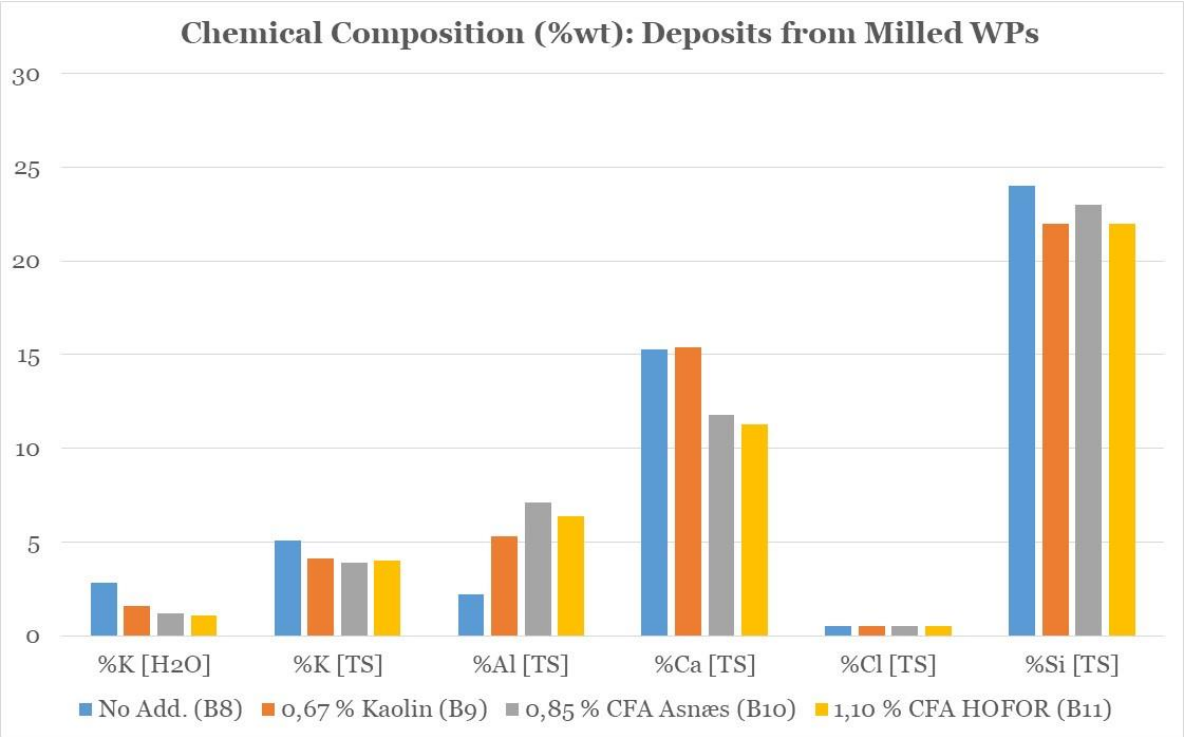

Figure 26: Chemical composition (based on ICP-AES) of deposits formed while firing milled wood pellets (fuel A1) with additives, in experiments B8-B11.

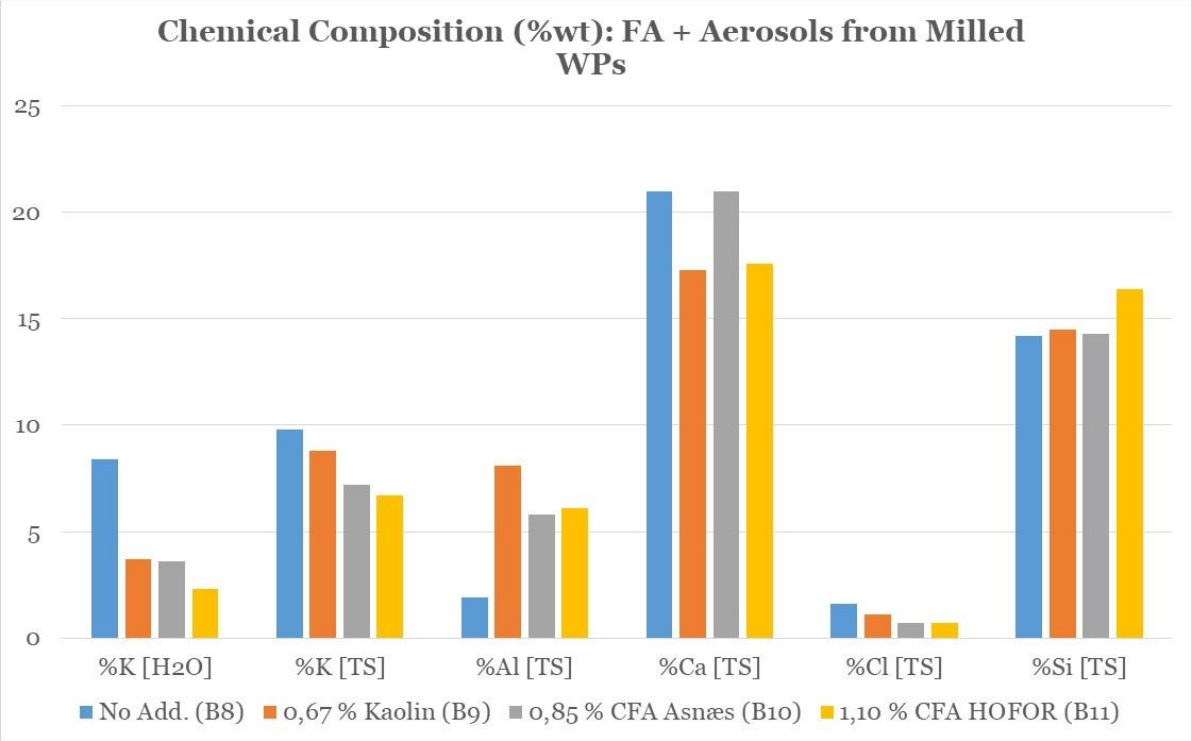

Figure 27: Chemical composition (based on ICP-AES) of fly ash + aerosols formed while firing milled wood pellets (fuel A1) with additives, in experiments B8-B11.

Figure 26-27 show the deposit and fly ash chemical composition, when firing fuel A and additives.

For the deposit data, Figure 26, changes are seen for H_2O-soluble [K] [decrease], as well as [Al] [increase]. For the two fly ashes, CFA Asnæs and HOFOR, there is also a significant reduction in [Ca] in the deposit, while this is not observed for Kaolin, which form deposits with a [Ca] similar to firing fuel A - milled wood pellets without an additive. For Si, no clear trend and effect of the use of additives, are seen.

For the fly ash chemical composition, a decrease in H_2O-soluble [K], total [K] and [Cl], is observed, see Figure 27. The decrease in H_2O-soluble K is more noticeable, with CFA HOFOR reducing it by 6,1%, while CFA Asnæs and Kaolin reduces it by 4,8% and 4,7%, respectively. The [Al] in the fly ash/aerosols increases due to the presence of the additive. No clear trends are seen in the [Ca]- respectively the [Si] of the fly ash/aerosols.

3.5. Influence of Additive Amount

Finally, the effect the additive dosage (amount) on deposit and fly ash compositions was investigated, by comparing data from experiment B1, B2 and B5.

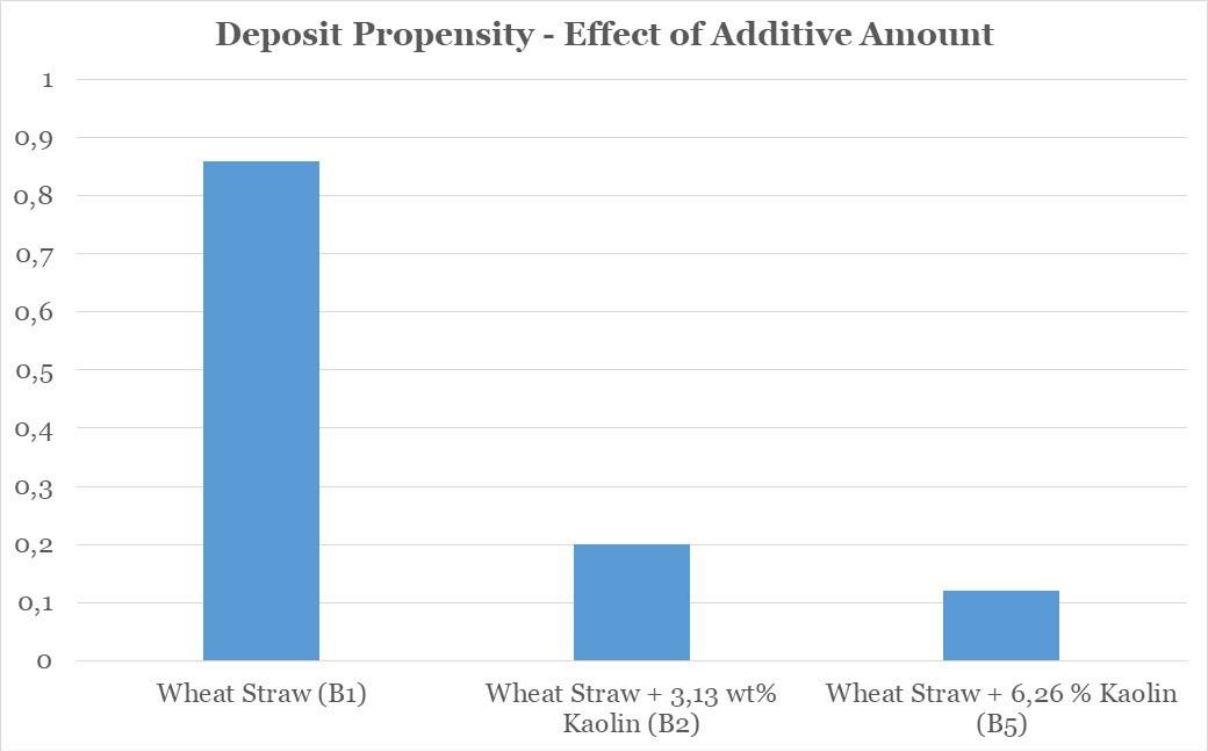

Figure 28: Deposit propensities for experiment B1, B2 and B5, illustrating the effect of additive amount dosed.

Experiment B1 was done with fuel D and no additives, experiment B2 was done fuel D with 3,13 wt.% kaolin, and experiment B5 was done with 6,26 wt.% kaolin.

From Figure 28 it is evident, that the additives reduces the deposit propensity. Increasing the additive dosage enhances the reduction. However, upon doubling of the additive dosage, the ash fed to the system also increases.

When looking at the fraction of H_2O-soluble [K] it can be seen in Table 9, that increasing the additive dosage decreases H_2O-soluble [K] in both deposit [69 % $\rightarrow$ 29 %] and fly ash [48 % $\rightarrow$ < 37 %]. This decrease is believed to be beyond the effect of dilution, and show that an enhanced reduction in H_2O-soluble [K] can be obtained by increasing the additive dosage [Naimi and Funch, 2019].

In Table 9 the K-conversion (X_K) and K-capture (C_K) for the regular, and double dosage kaolin experiments, are shown. The K-conversion increases [31 % → > 70 %], when using additives. This is attributed to the increase in available aluminosilicate, supplied by the double additive dosage. However, due to the increase in additive dosing, the overall K-capture efficiency of the Kaolin additive is reduced from 0.28 gram H_2O soluble K per gram additive, to 0.24 gram H_2O soluble [K] per gram additive, see Table 9.

Table 9: Fraction of H2O-soluble [K] detected in deposit and fly ash, fraction of aerosols of the total fly ash, and K-conversion (XK) and K-capture (CK) for experiments B1, B2 and B5 [Naimi and Funch, 2019].

Fuel fed	**H_2O-sol K Deposit (%)**	**H_2O-sol K Fly ash (%)**	**% Aerosols**	**K-Conversion, X_K**	**K-Capture, C_K**
Fuel D, no additive: (B1)	48	69	17	31	NR
Fuel D, 3.13 wt. % Kaolin (B2)	37	29	13	70	0,28
Fuel D, 6.26 wt. % Kaolin (B5)	15	15	10	85	0,24

Looking at the detailed chemical composition of the deposit, Figure 29, it becomes evident that the increased additive dosage have a beneficial impact on the deposit and fly ash composition. For the deposit, the H_2O-soluble as well as the total [K] is reduced. This effect is attributed to the additional available aluminosilicate, from the double dosage, available for reactively capture of the K.

Concerning the fly ash/aerosols, again both the H_2O-soluble and the total [K] decreases, as does [Ca] and [Cl], while there is a significant increase in the A-content, which was to be expected. No obvious trends are seen for Si, see Figure 30.

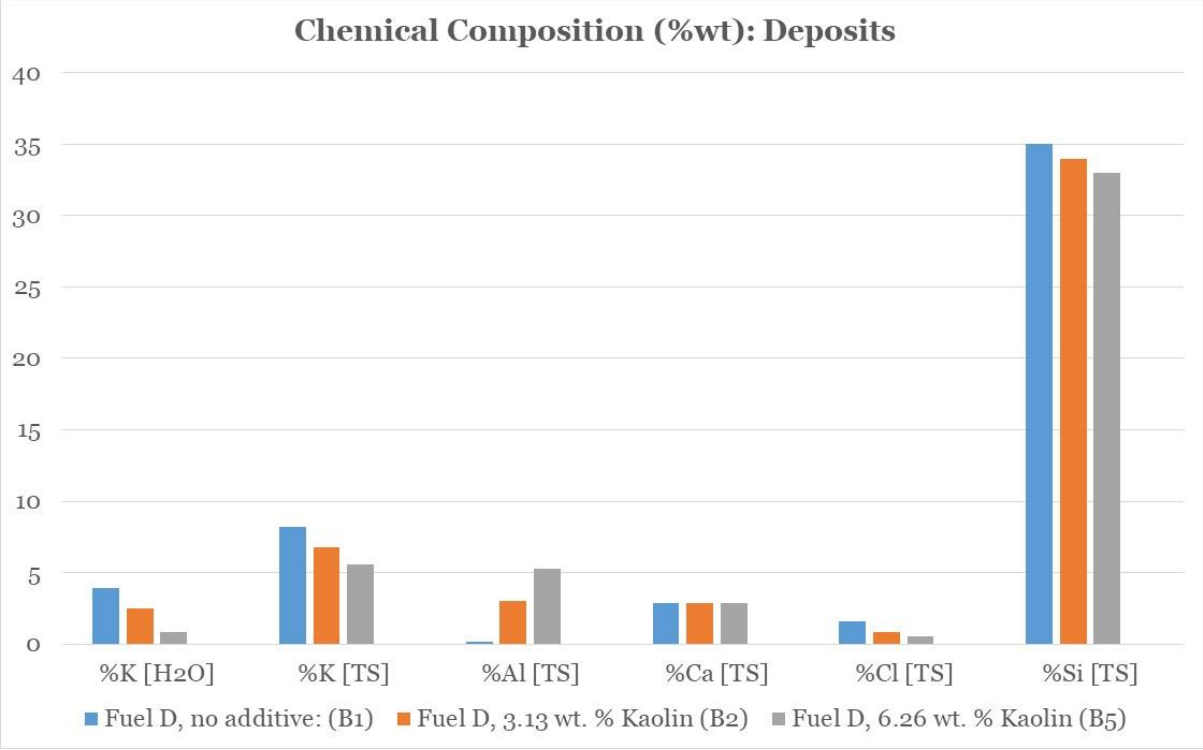

Figure 29: Chemical composition (based on ICP-AES) of deposits formed while firing straw (fuel D) with various amounts of additives, in experiments B1, B2 and B5.

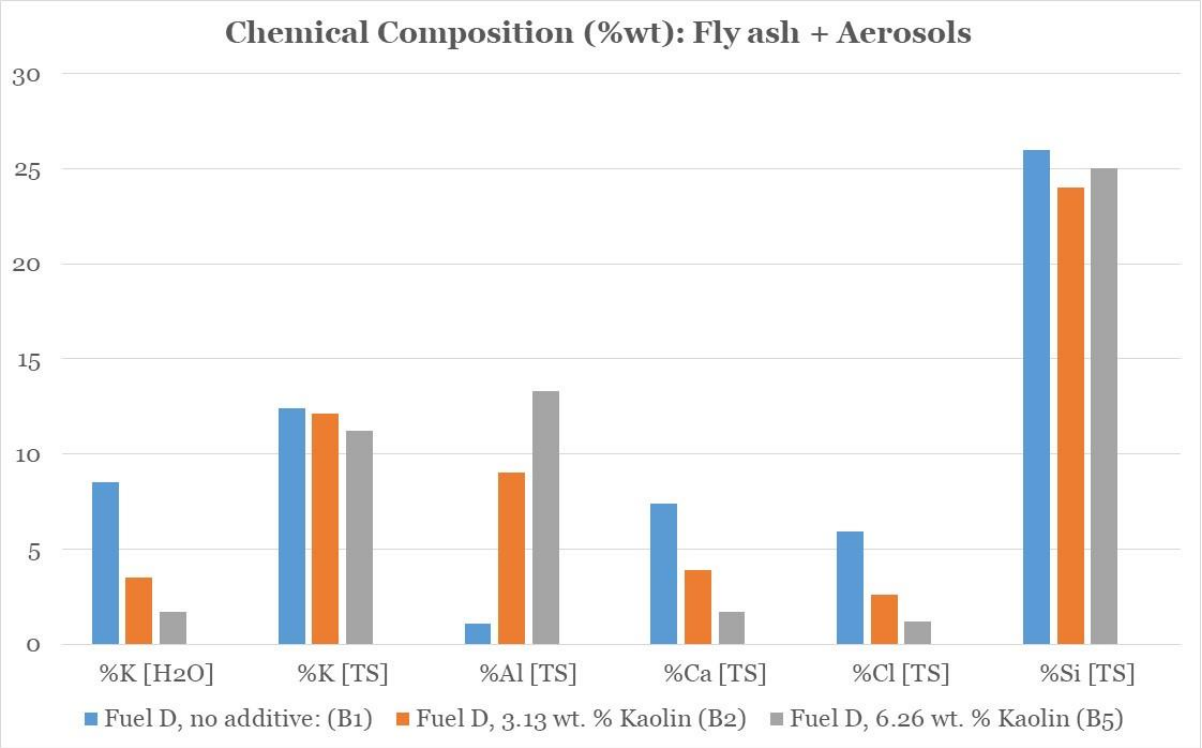

Figure 30: Chemical composition (based on ICP-AES) of fly ash + aerosols formed while firing straw (fuel D) with various amounts of additives, in experiments B1, B2 and B5.

4. XRD Analyses

ICP-analyses provide an elemental composition of an ash sample, but basically no information about how the elements are chemically associated in the sample. For this purpose, X-Ray Diffraction (XRD) analysis, is a very efficient tool, provided that the sample contain crystalline phases.

All cyclone, filter and deposit samples collected as part of this measuring campaign, were analyzed by XRD.

Figure 31 show a XRD-diagram of the cyclone sample from Experiment B1, revealing that the sample is rich in CaO, SiO_2, but also contain traces of KCl. K_2SO_4 was not detected in the cyclone sample although it exists in filter and deposit samples. $K_2Si_4O_9$ is not detected, although it was predicted by equilibrium calculation [Wang, 2018].

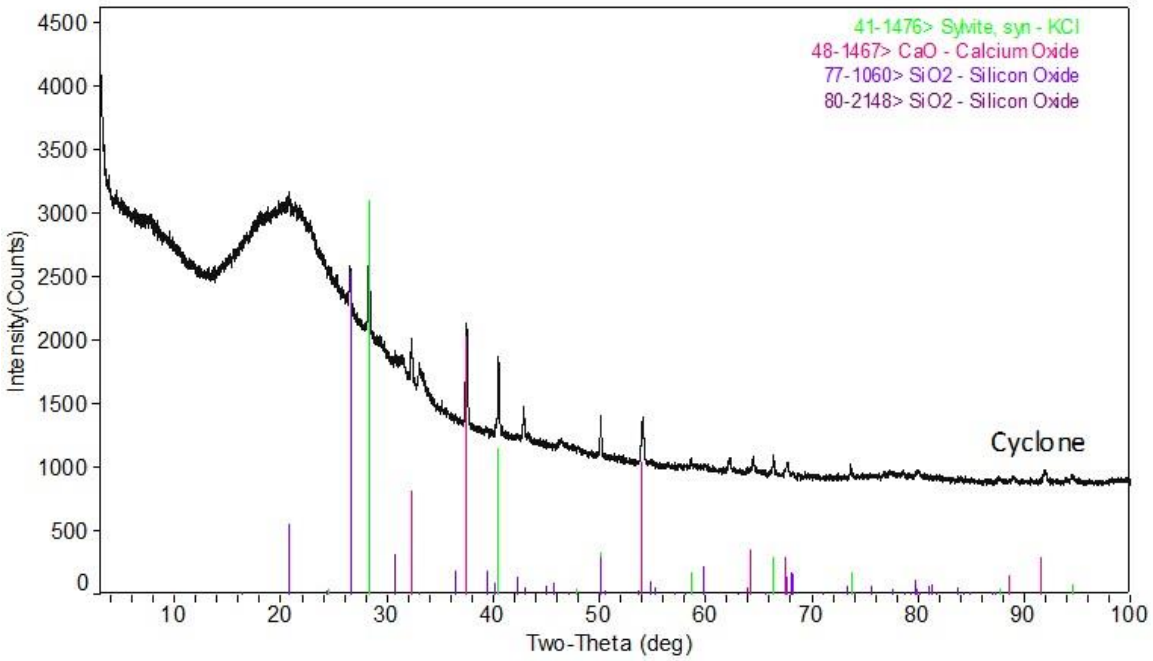

Figure 31: XRD-diagram of cyclone ash from experiment B1 – Wheat Straw without additive.

Peaks in XRD-diagram of the filter sample were much stronger than those in cyclone. Main peaks are from KCl and K_2SO_4, which are the most problematic species. Stronger peaks indicate a high concentration of KCl and are fairly crystalized.

Figure 33 show XRD-diagrams of up- respectively downstream deposits from experiment B1, Straw-firing without additive. Both samples are dominated by KCl and K_2SO_4, the peaks of which are much stronger in the downstream sample, than in the upstream sample.

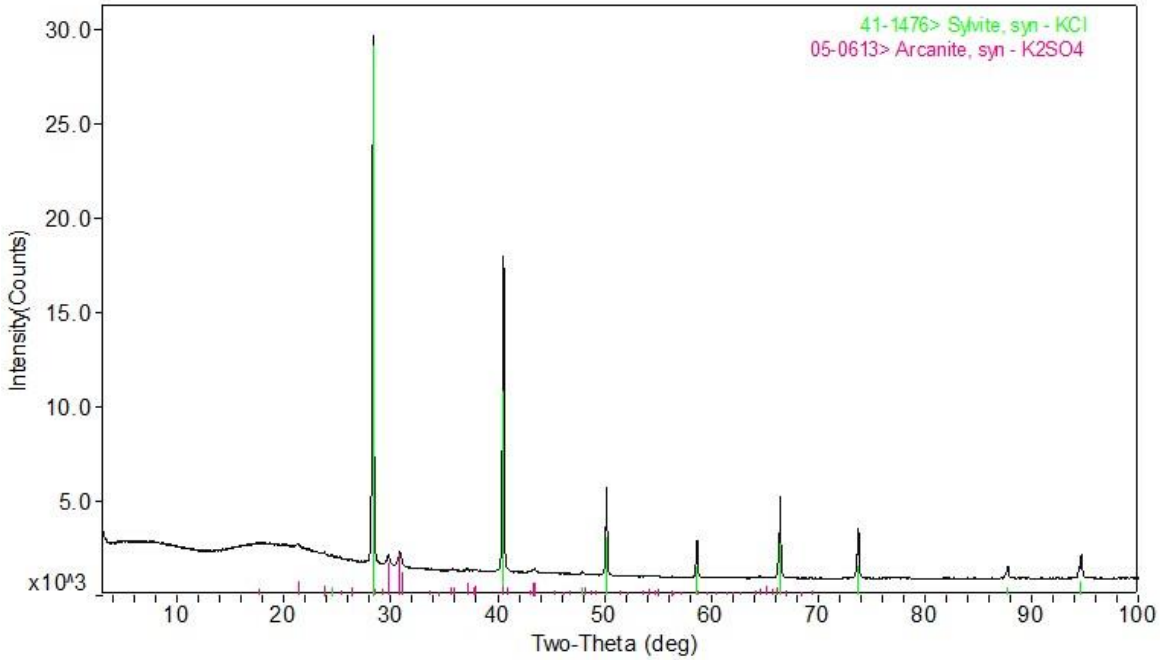

Figure 32: XRD-diagram of filter ash from experiment B1 – Wheat Straw without additive.

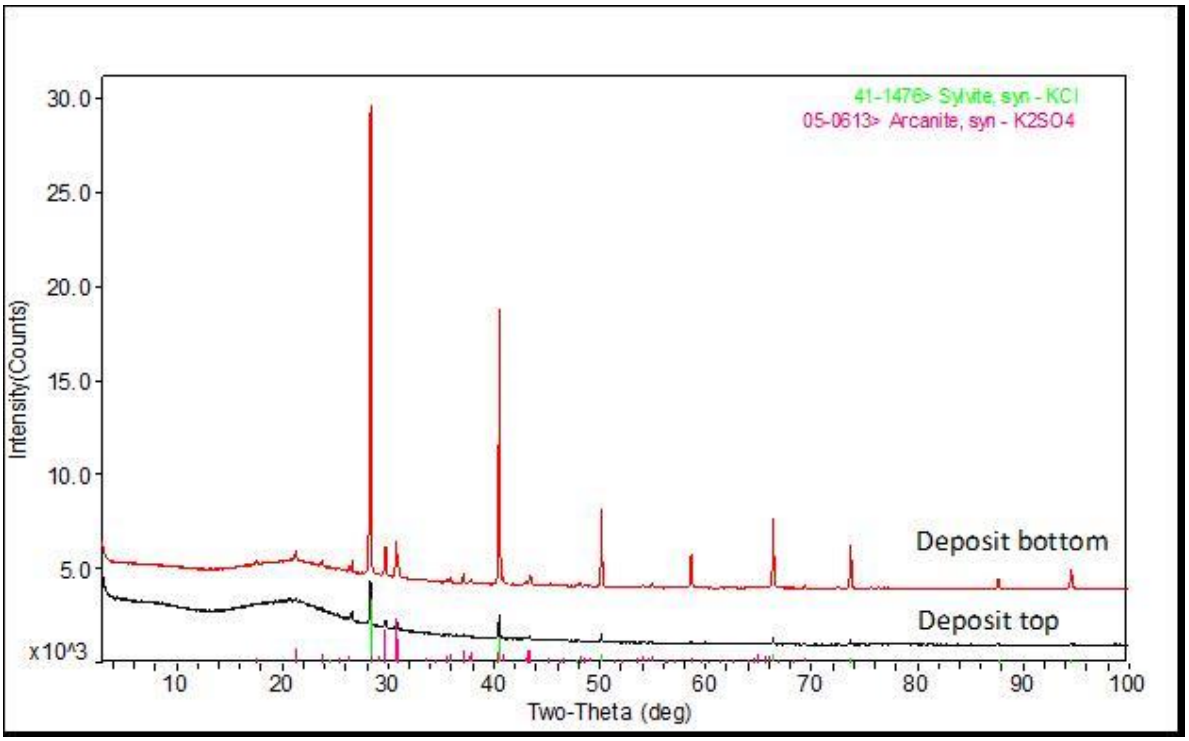

Figure 33: XRD-diagram of up- respectively downstream deposits from experiment B1 – Wheat Straw without additive.

Table 10: Summary of XRD-finding in samples from experiment B1 – Wheat Straw without additive.

Exp. B1 Wheat Straw without additive				
	Cyclone	Filter	Deposit top	Deposit bottom
SiO_2	X			
CaO	X			
KCl	X	X	X	X (very strong)
K_2SO_4		X	X	X

Similar identification of crystalline phases were done for all the samples collected. In Figure 34, a comparison between crystalline phases identified in samples from experiment B6 – HTC Leaves without additive, is shown.

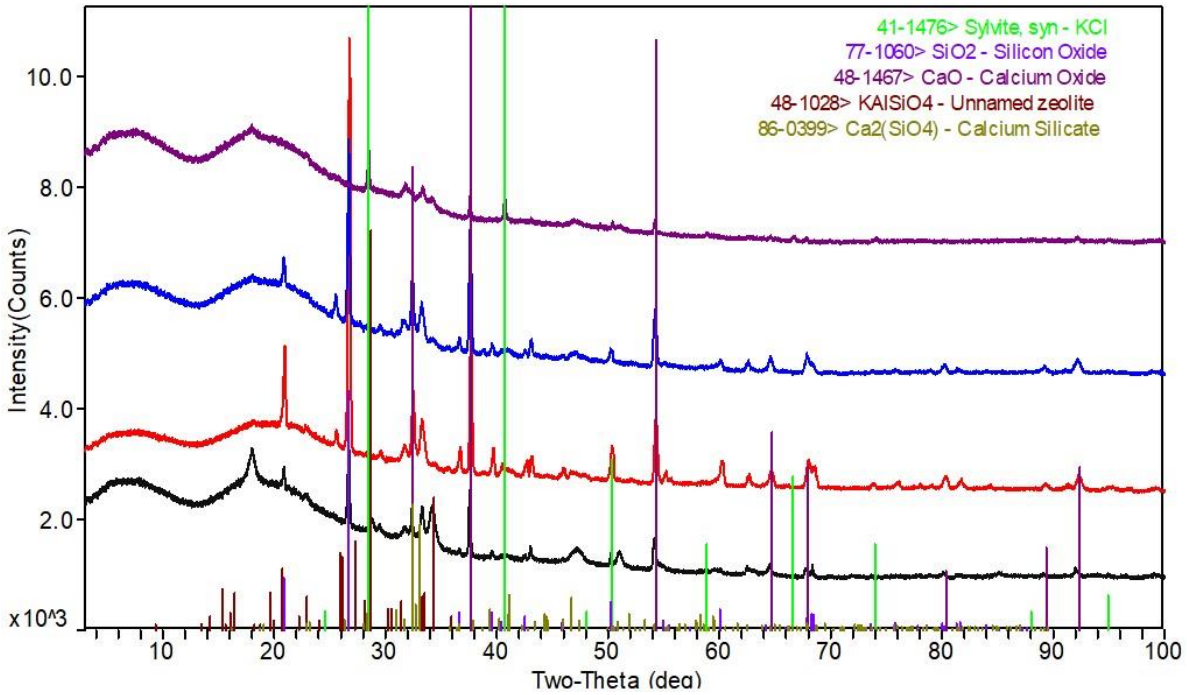

Figure 34: XRD-diagram of samples, i.e. cyclone, filter, deposit top and deposit bottom, from experiment B6 – HTC Leaves without additive.

In Table 11, it is seen that also phases with chemical interaction between Ca, K, Al and Si have been identified in the XRD-analysis.

In general, several of the XRD-diagrams reveal especially the presence of KCl, but also K_2SO_4, and in many cases especially in cyclone ash samples of samples from upstream deposits, also SiO2 and CaO are present in significant amounts.

Table 11: Summary of XRD-finding in samples from experiment B6 – HTC Leaves without additive.

Exp. B6 HTC leaves				
	Cyclone	Filter	Deposit top	Deposit bottom
SiO_2	X		X	X
CaO	X	X	X	X

KCl		X		
K_2SO_4				
$KAlSiO_4$	X			
Ca_2SiO_4	X		X	X

The XRD-analysis reveal the main deposit formation on the upstream side to be inertial impaction, while small aerosol-size particles rich in KCl and K_2SO_4 are dragged in by eddies on the back side of the deposition probe, forming a very thin layer, rich in K, Cl and S.

Not many mineral species containing K and Al, Si, Ca together are identified in the XRD-analyses, indicating that the main effect of the additive is to provide surface for condensation of volatile K-species, thereby not causing problems in the deposit.

5. SEM Analysis of Deposit Samples

Deposit samples from wheat straw combustion with kaolin and without kaolin addition were analyzed by SEM. The experimental conditions are listed below.

Table 12: Experimental conditions for experiment B1 and B2.

Exp.	Temperature	Fuel	Additive	Samples analyzed
B1	1350 °C	Wheat straw	No additive	Cross sectional deposit
B2	1350 °C	Wheat straw	3.13 % kaolin	Cross sectional deposit Brushed off deposit (bottom and top), filter sample

Two cross sectional deposit specimens were analyzed. One was from EFR experiment B1, where wheat straw was combusted without kaolin addition. The other specimen is from experiment B2 where wheat straw was combusted with 3,13 % kaolin added, as K-capture additive.

After each experiment, deposit sitting on the deposition probe was glued, cut and polished in order to get a cross sectional specimen. The specimen was then analyzed by SEM-EDX at DTU-CEN (Center for Electron Nanoscopy). During polishing, 96% Ethanol was applied, which may result losing of the water soluble K species [Even with 100% Ethanol polishing, it is still difficult to avoid losing the water soluble K-species, since it can be easily flush away]. Therefore, all the K detected by EDX, is water-insoluble.

Additionally, deposit was brushed off and collected in another - repeated - experiment at the same conditions as B2. Samples collected from filter together with the brushed off sample, were subjected to SEM-EDX analysis.

What should also be emphasized here is that the deposit sitting loosely on the top, and the deposit closely attached to the probe [inner layer], were collected separately, and were named as deposit top and deposit bottom respectively.

The SEM images are summarized in Figure 35. SEM images were obtained for particles located closely to the deposit probe, particles in the middle of the deposit, as well as the particle at the top of the deposit.

Comparing Figure 35(A) and (B), the size of the particles is similar. However, more spherical particles are observed in Figure (B), which is obtained from wheat straw combustion with kaolin addition.

The SEM-EDX results of cross sectional deposit, sitting on probe from experiment B1 (wheat straw combustion without kaolin) are shown in Figure 36. The results show that the ash particles are rich in Si, K and Ca, while the content of Al is only 1,1 %. This is because the parent fuel, wheat straw has a low Al-content. The content of K is much lower than that of wheat straw. What should also be noticed, is that no Cl was detected in the specimen. The content of S is also very low, only 0,3 %. This is most likely because the water-soluble KCl and K_2SO_4 has been washed out. In the B2 specimen (with kaolin addition), similar results have been observed.

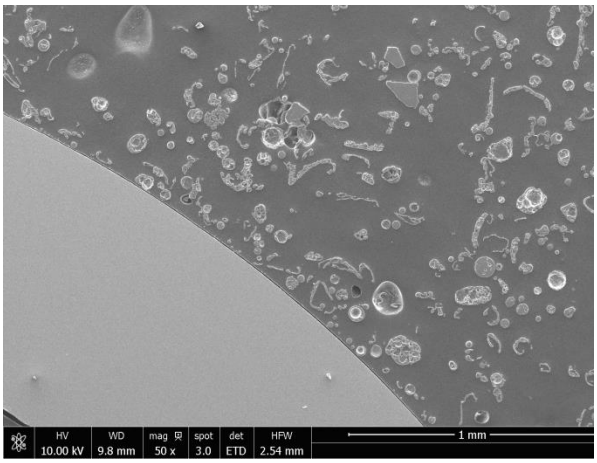

(A) Near the deposit probe, 50 X, **with** kaolin

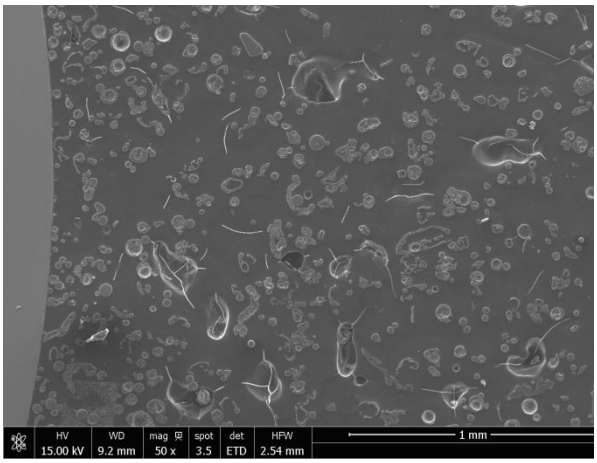

(B) Near the deposit probe, 50 X, **without** kaolin

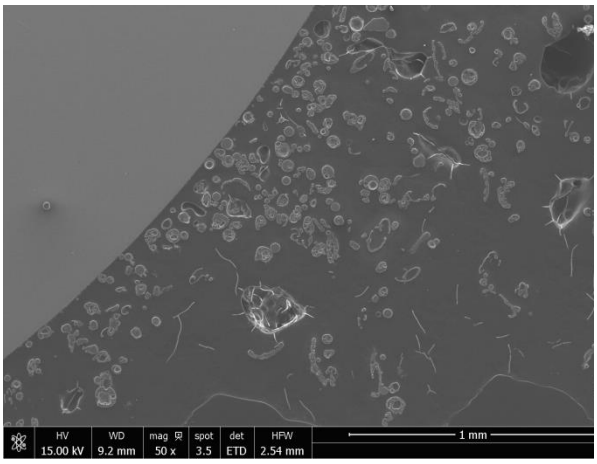

Near the deposit probe, 50 X, **without** kaolin

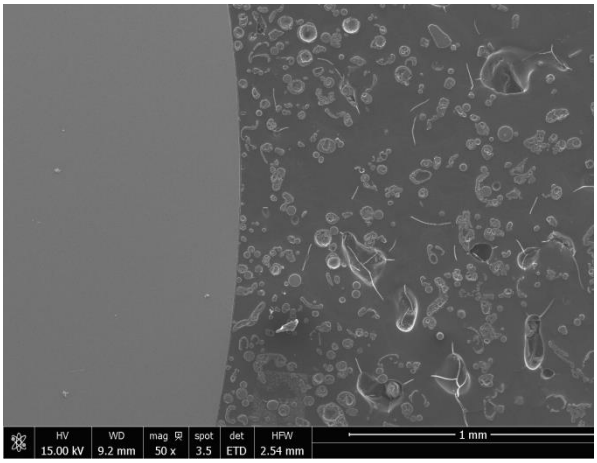

Near the deposit probe, 50 X, **without** kaolin

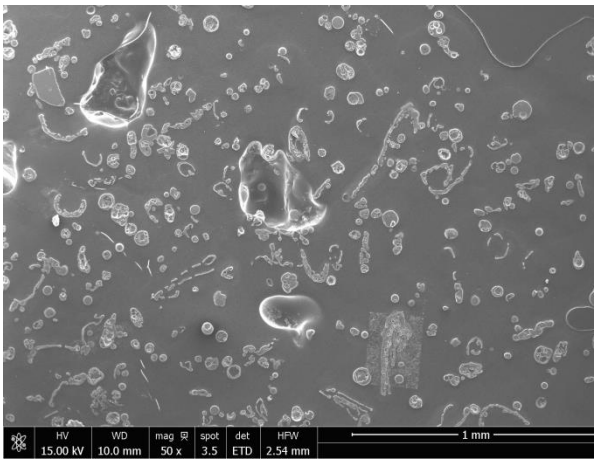

At the top of deposit, 50 X, **without** kaolin

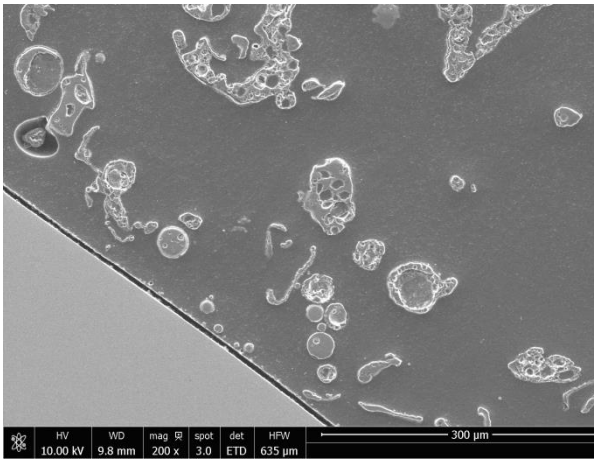

Near the deposit probe, 200 X, **with** kaolin

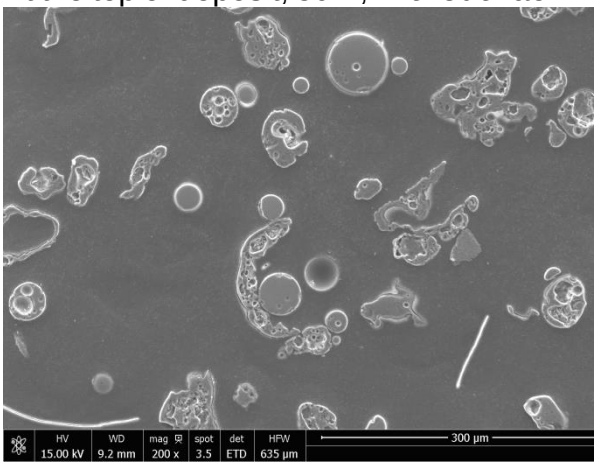

Near the deposit probe, 200 X, **without** kaolin

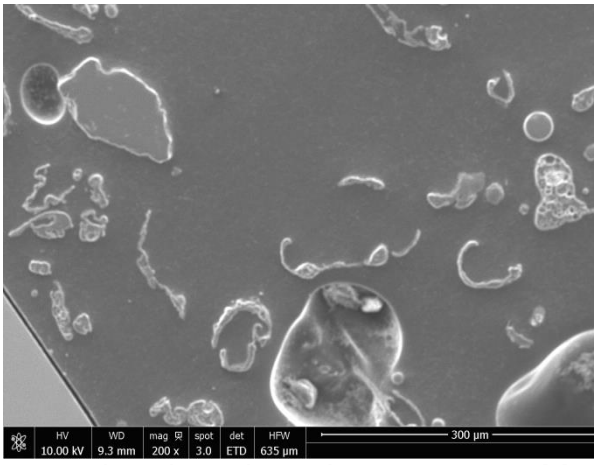

Near the deposit probe, 200 X, **with** kaolin

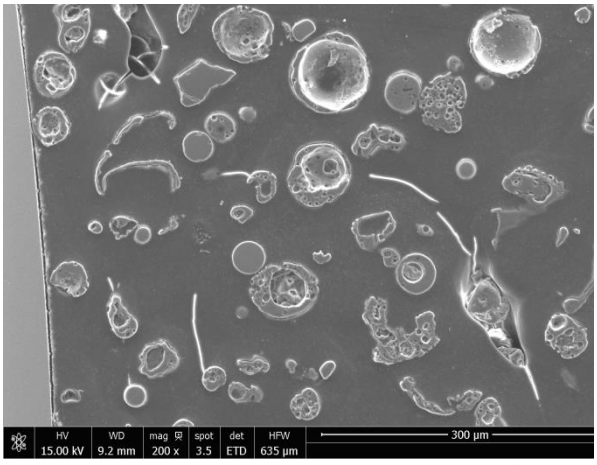

Near the deposit probe, 200 X, **without** kaolin

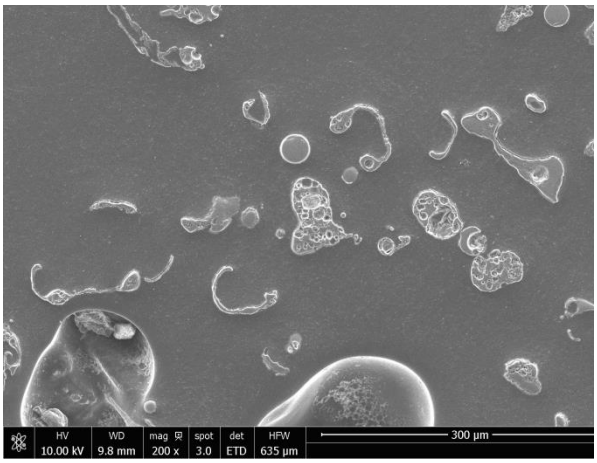

Near the deposit probe, 200 X, **with** kaolin

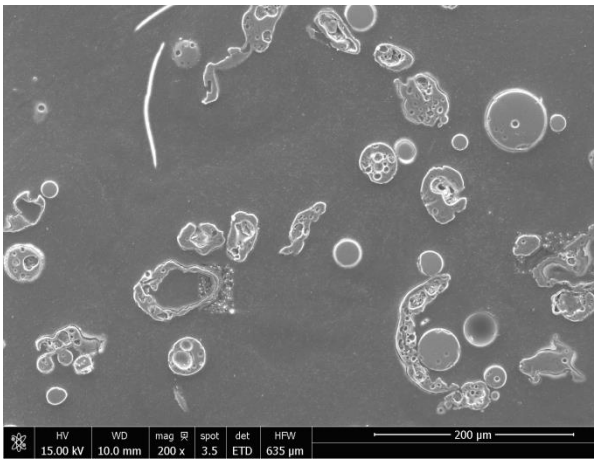

Near the deposit probe, 200 X, **without** kaolin

Near the deposit probe, 500 X, **with** kaolin

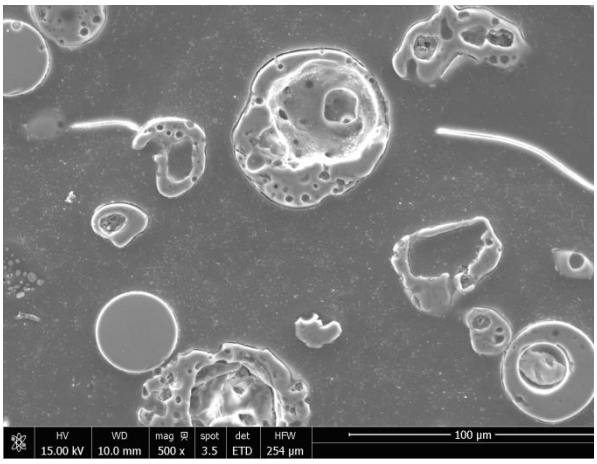

Near the deposit probe, 500 X, **without** kaolin

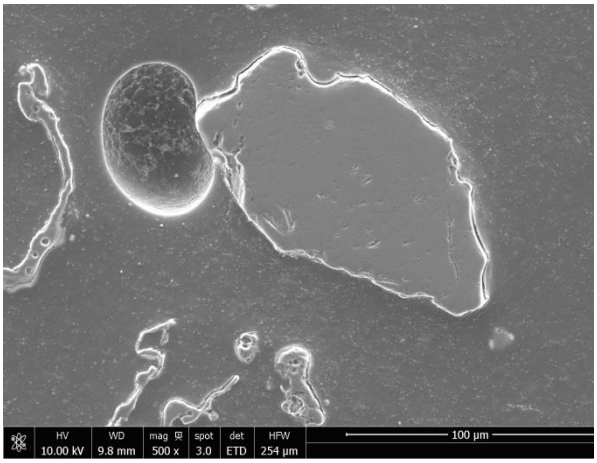

Near the deposit probe, 500 X, **with** kaolin

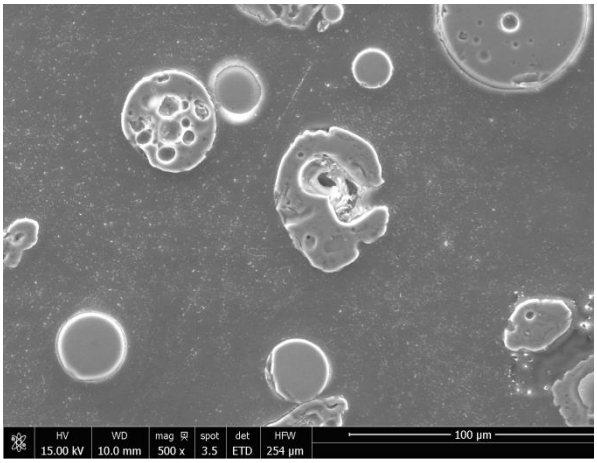

Near the deposit probe, 500 X, **without** kaolin

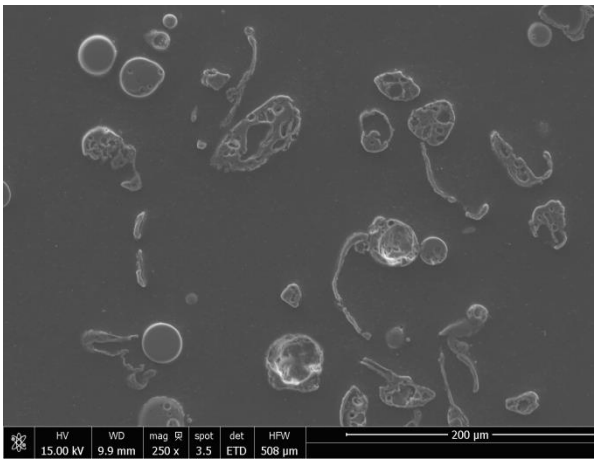

In the center of deposit, 250 X, **with** kaolin

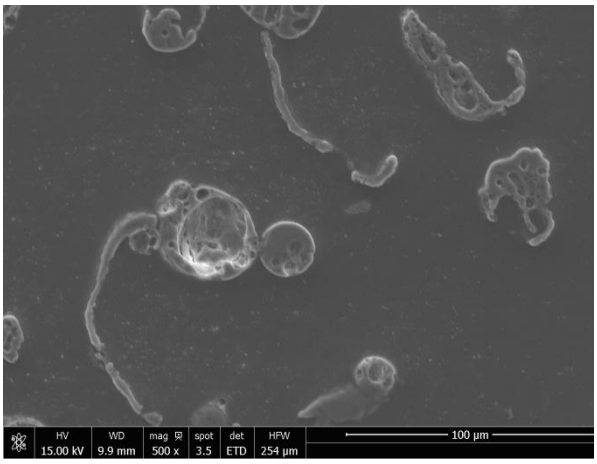

In the center of deposit, 500 X, **with** kaolin

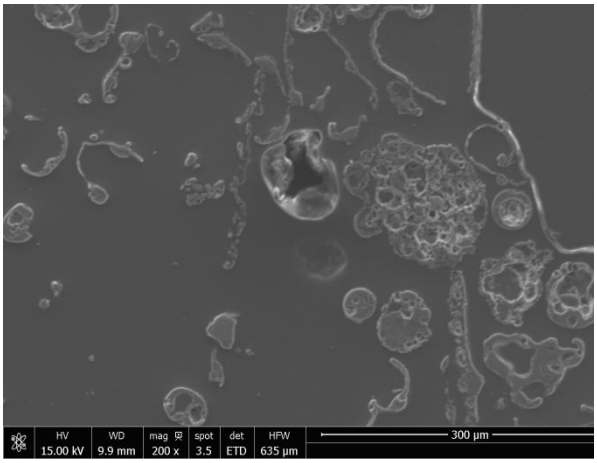

On the top of the deposit, 200 X, **with** kaolin

Figure 35: Ash deposit formed on the EFR deposit tube, during wheat straw combustion.

A significant of Cl was detected in the brushed off bottom deposit (Figure 35).

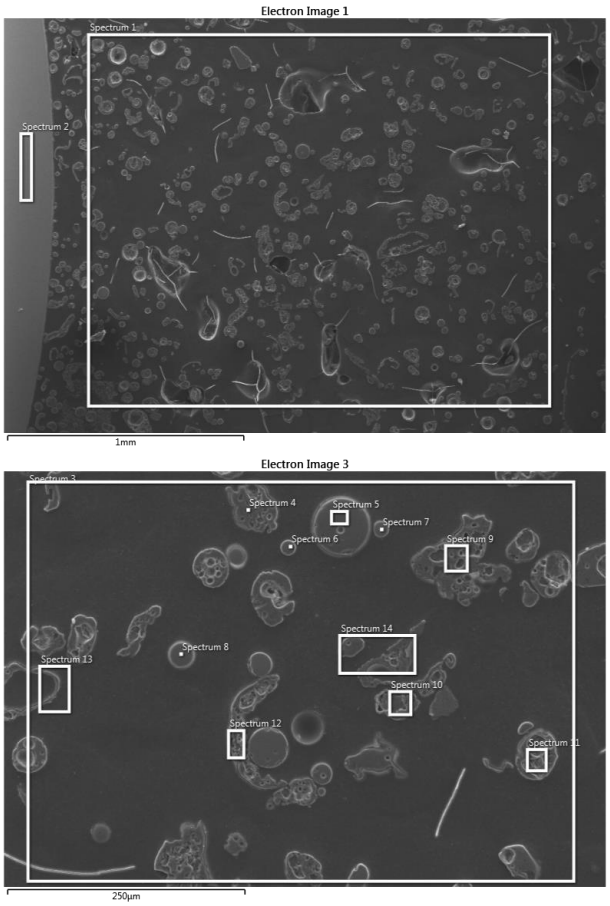

(A) SEM images

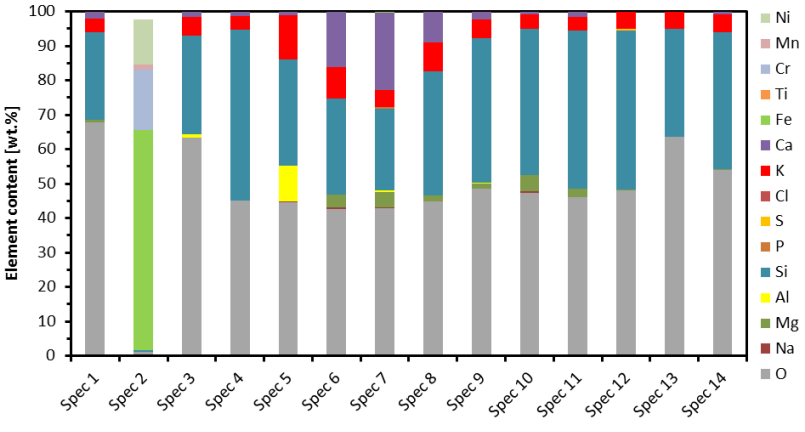

(B) Element content of each spectrum

Element	content wt.%
O	49.71
Na	0.10
Mg	1.71
Al	1.11
Si	35.91
P	0.06
S	0.03
Cl	0.00
K	6.29
Ca	5.04
Fe	0.04
Ti	0.00
Cr	0.00
Mn	0.00
Ni	0.00

(C) average of all spectra **except spectrum 2**

Figure 36: SEM-EDX results of cross sectional deposit sitting on deposit probe from EFR experiment B1 (wheat straw combustion without kaolin).

The SEM-EDX results of cross sectional deposit sitting on probe from experiment B2 (wheat straw combustion with kaolin), are shown in Figure 37.

The ash particles are rich in Si, K, Ca, and Al. The higher contents of Si and Al in this sample, are due to the addition of kaolin as additive.

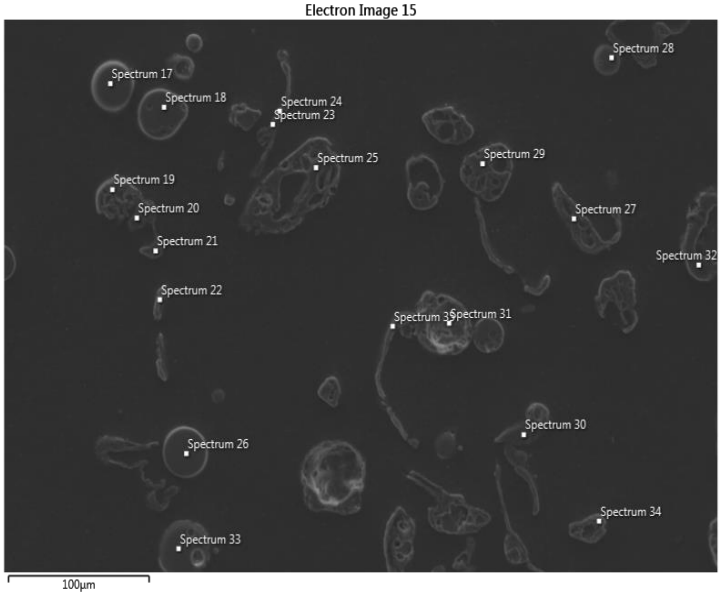

(A) SEM image

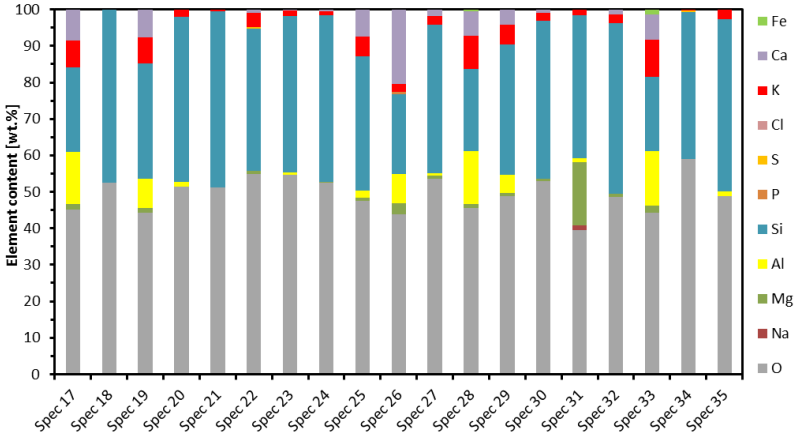

(B) Element content of each spectrum

Element	content wt. %
O	49.40
Na	0.07
Mg	1.67
Al	3.77
Si	37.84
P	0.03
S	0.04
Cl	0.00
K	3.52
Ca	3.56
Fe	0.10

(C) average of all spectra

Figure 37: SEM-EDX results of deposit sitting on probe from EFR experiment B2 (wheat straw combustion with kaolin).

The SEM-EDX results of brushed off deposit **bottom and top** samples, are summarized below, Figure 38-39. The sample is dominated by spherical particles. Some long shape ash particles, maintaining the original shape of wheat straw, can also be seen. Some flaky particles were noticed to have a significant high content of K and Cl (spectrum 6, 14, 15, 21, 33, 37). The flaky particles were probably KCl, which formed on the deposit probe surface, and were then brushed off during sample collection.

What should also be noticed, is that the average content of K is much higher than that in the cross sectional deposit samples.

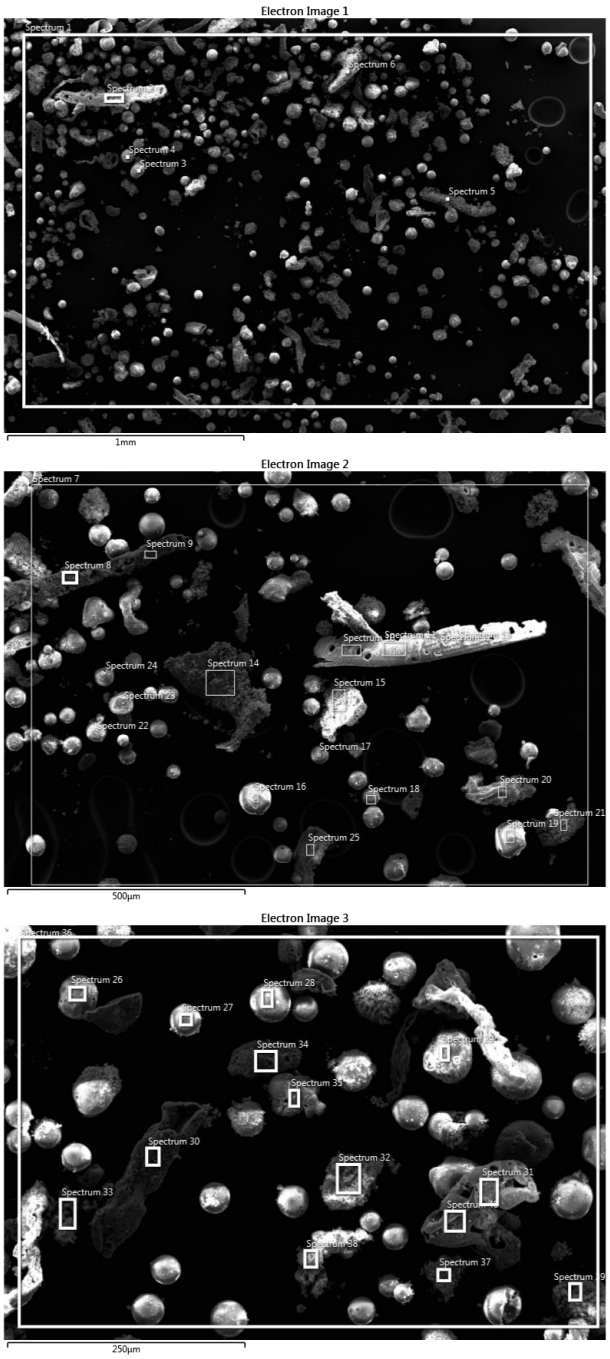
Electron Image 1
Spectrum 1
Spectrum 6
Spectrum 4
Spectrum 3
Spectrum 5
1mm
Electron Image 2
Spectrum 7
Spectrum 9
Spectrum 8
Spectrum 24
Spectrum 14
Spectrum 15
Spectrum 23
Spectrum 22
Spectrum 17
Spectrum 16
Spectrum 18
Spectrum 20
Spectrum 21
Spectrum 19
Spectrum 25
500µm
Electron Image 3
Spectrum 26
Spectrum 28
Spectrum 27
Spectrum 34
Spectrum 35
Spectrum 30
Spectrum 32
Spectrum 31
Spectrum 33
Spectrum 37
250µm

(A) SEM images

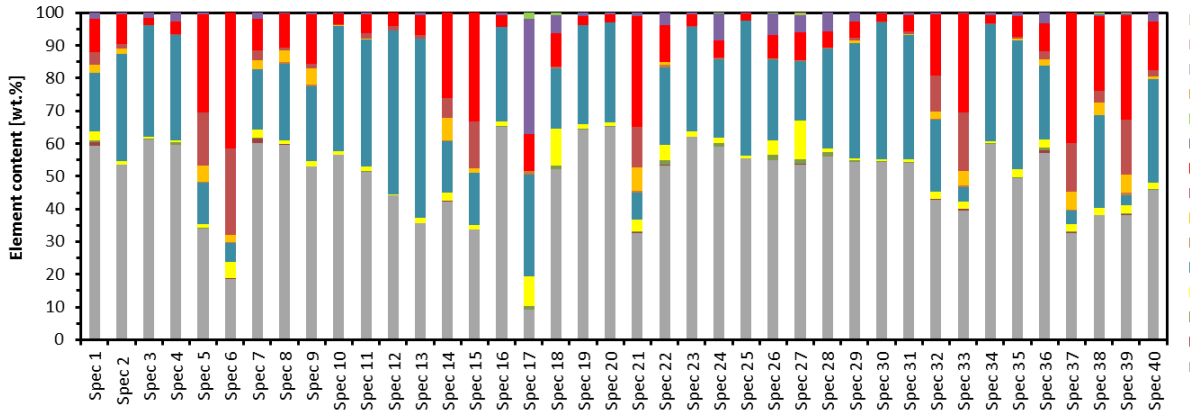

(B) Element content of each spectrum

Element	content wt. %
O	48.93
Na	0.14
Mg	0.40
Al	2.51
Si	26.63
P	0.19
S	1.60
Cl	4.18
K	12.80
Ca	2.51
Fe	0.11
Ti	0.00
Cr	0.00
Mn	0.00
Ni	0.00

(C) average of all spectra

Figure 38: SEM-EDX results of deposit bottom brushed off deposit probe from EFR experiment B2 (wheat straw combustion with kaolin).

The brushed off deposit top sample, is shown in Figure 39. The sample is dominated by long ash particles, and the K- and Cl-content is relatively lower than that of the bottom deposit.

The filter sample results are shown in Figure 40. The sample is primarily composed of particles below 2 µm.

The K content is as high as 22%. And Cl is 13 %.

In the sample, the relatively bigger particles are probably reacted kaolin particles, with a similar content of Si, Al and K ($KAlSiO_4$ has been detected in previous study), and Cl is very low. The smaller particles could be a mixture of unreacted KCl and Si, Al from fuel or additive, since it has a higher Cl content and the K content is higher than that of Al and Si.

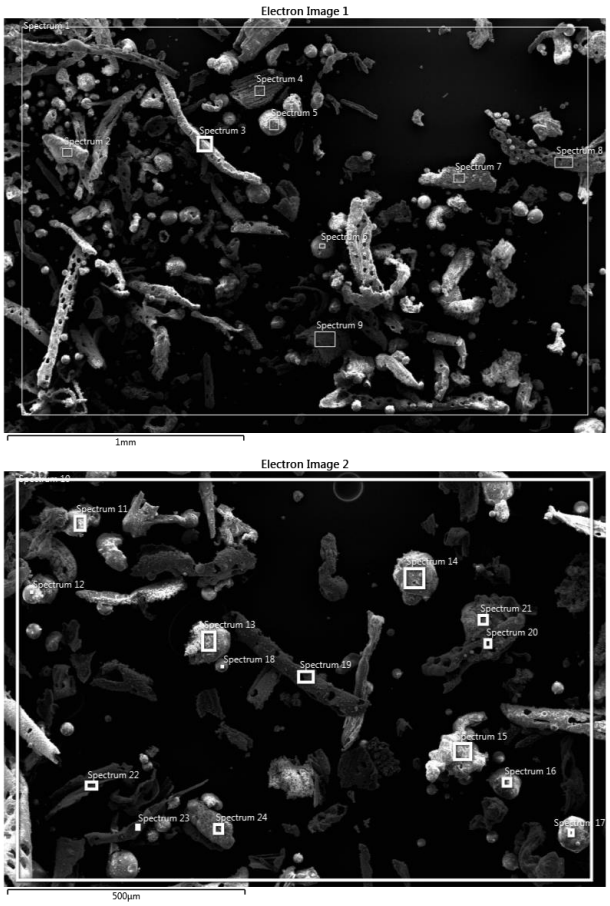

(A) SEM images

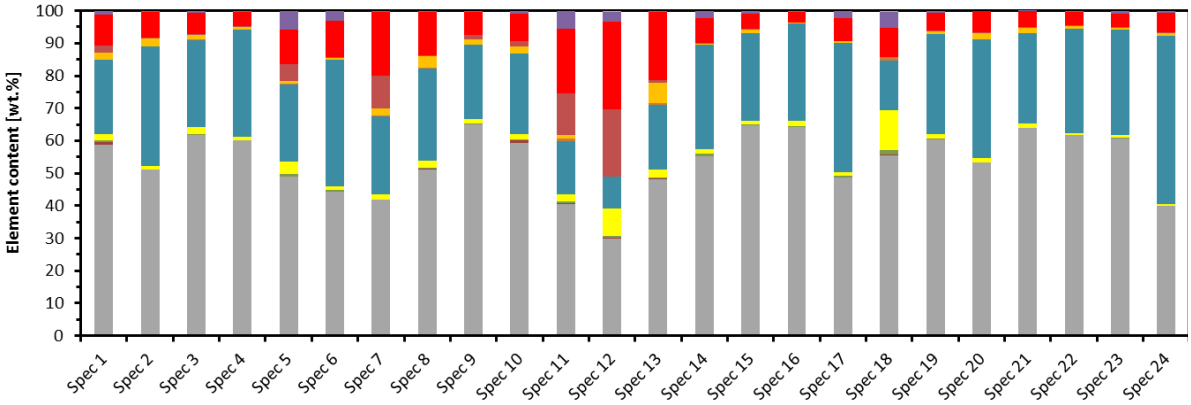

(B) Element content of each spectrum

Elements	content wt. %
O	53.60
Na	0.12
Mg	0.37
Al	2.32
Si	28.37
P	0.18
S	1.29
Cl	2.52
K	9.64
Ca	1.57
Fe	0.03
Ti	0.00
Cr	0.00
Mn	0.00
Ni	0.00

(C) average of all spectra

Figure 39: SEM-EDX results of deposit top brushed off deposit probe from EFR experiment B2 (wheat straw combustion with kaolin).

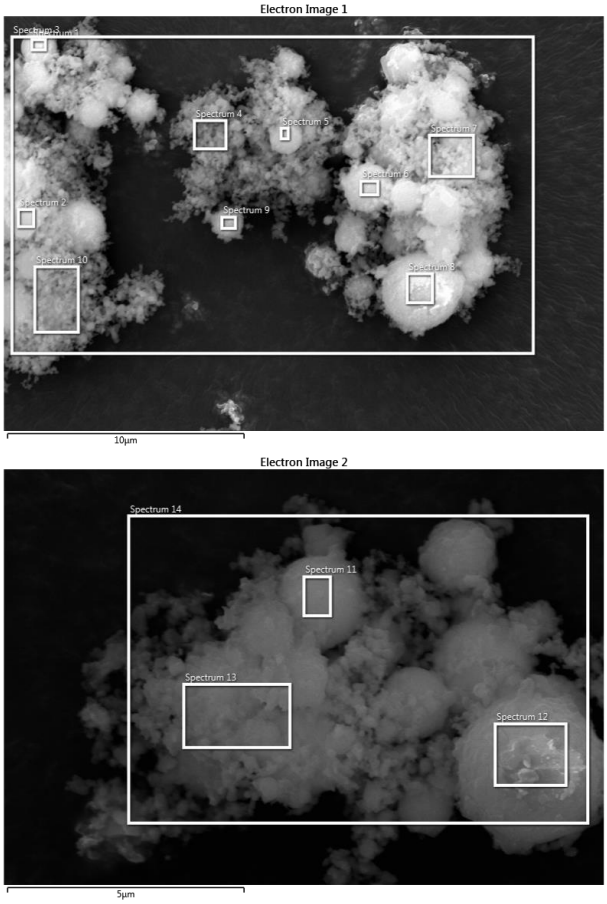

(A) SEM images

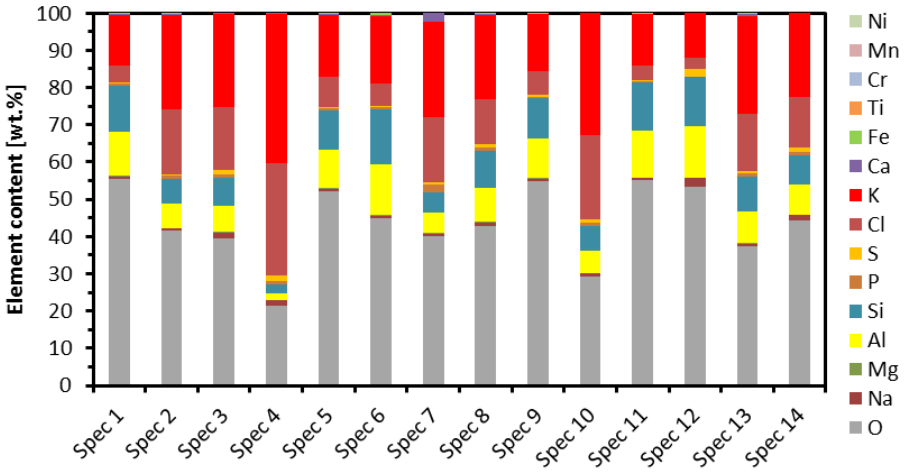

(B) Element content of each spectrum

O	43.77
Na	0.94
Mg	0.14
Al	8.93
Si	9.32
P	0.81
S	0.73
Cl	12.69
K	22.14
Ca	0.33
Fe	0.18
Ti	0.00
Cr	0.00
Mn	0.00
Ni	0.00

(C) average of all spectra

Figure 40: SEM-EDX results of filter sample from EFR experiment B2 (wheat straw combustion with kaolin).

6. Summary and Conclusions

This measuring campaign has provided a set of high-quality data for simulation deposit formation in systems fired with biomass in suspension, utilizing additives for K-capture.

Four biofuels were selected for the measurements; milled wood pellets, HTC Leaves, SE Bark, and, a high-K Danish Wheat Straw. The first three of these fuels were Biofficiency fuels, tested also by other partners in other technologies. The Danish wheat straw was selected due to it high level of K, and known tendency to cause deposit problems. It was taken from the DTU fuel storage, and is the same fuel as utilized by [Damoe et al., 2017], in their studies of fly ash formation.

Three additives were defined by Biofficiency partners for the tests, a Kaolin and two Coal Fly Ashes (CFAs).

Milled wood pellets and wheat straw were fired alone, as well as with each of the three additives, while the wheat straw was also with different Kaolin dosing, in order to test the effect of additive dosing. HTC leaves and SE bark did not cause much deposit formation, when fired alone and where therefore not tested with the additives.

Samples collected were analyzed by ICP-AES, XRD and SEM.

The data from the measurements showed a pronounced effect of the additives on deposit propensity, the additive amount being of greater importance than the type (chemistry) of the additive. Chemical analyses (ICP and XRD) revealed a lot of K, Cl and S – but also substantial amounts of Ca and Si in some samples.

The utilizing an additive together with Danish Wheat Straw, the deposition propensity decreased from ~ 80 % to ~ 20 %, i.e. a substantial decrease in the deposit formation tendency. This is due to the capturing of K by the additive, thereby preventing K from making deposits and fly ash particles as sticky as when fired without an additive. Both Kaolin and the two CFAs showed this effect.

When firing milled wood pellets the opposite was observed, i.e. the deposition propensity increased from ~ 12 % to 15-20 %. Not a very dramatic increase, but this is caused by the fact that milled wood pellets have a rater low ash content, therefore adding an additive will increase the ash flux in the system, and, thereby, also the increase of deposited ash particles (i.e. the deposition propensity).

Fuel Type:

On the effect of fuel type, a comparison of deposit and fly ash/aerosol chemistry from the four different fuels, revealed a similar chemical composition of deposit and fly ash/aerosols for the same fuel. For all fuels [Ca] was higher in the fly ash/aerosols compared to the deposit, while the opposite was found for [Si] (i.e. higher in deposits compared to fly ash aerosols).

Additive Type:

Concerning the influence of additive type, in the case of Danish wheat straw firing, both kaolin and CFA gave a significant reduction in the deposition propensity, but when dosed in similar amounts (~3 %), the CFA gave lower deposition propensity than kaolin. Only when dosed in the double amount (~ 6%) kaolin caused a reduction similar to the CFAs in deposition propensities. For the CFAs no effect was observed from doubling the dose of additive.

Chemically, Kaolin gave by far the highest X-conversion (70 %) compared to 45-63 % for the two CFAs. Kaolin also had the highest K-capture of the three additives tested. All three additives cause lower total as well as water-soluble [K] in deposits, fly ashes and aerosols.

In the case of milled wood, increasing the amount of additive from 0,67 % to 1,10 % increased the deposition propensity from 15 % to 20 %. All the additives caused significant increase in the K-conversion, from 16 % for the 'pure' fuel (milled wood pellets) to 51-66 %, when an additive was applied. Kaolin had a higher K-capture than both CFA Asnæs and CFA HOFOR.

Chemically, total [K] and [Si] decreased when firing straw with increasing amounts of Kaolin/CFA. [Al] increased for obvious reasons. In the fly ash/aerosols there where a reduction in total [K], when utilizing Kaolin/CFA. A reduction was also observed in [Ca] and [Cl], in the fly ash/aerosols, probably due to dilution of the fly ash/aerosol by Al from the additive.

In the case of milled wood, again total and water-soluble [K] and [Cl] are decreased in the fly ash/aerosols, while only water-soluble [K] is decreased in the deposits. [Al] is significantly increased, especially in the fly ash/aerosols, compared to firing 'pure' milled wood.

Additive Amount:

The deposition propensity decreases significantly when adding Kaolin [86 % → 15-20 %], but the reduction in deposition propensity caused by doubling the additive dose from 3,13 % to 6,26 % was more moderate [20 % → 12 %].

A substantial reduction in water-soluble [K] was observed both in the deposit [48 % →15 %, fly ash [69 %→15%] and aerosols [17%→10%], when applying the highest dose of kaolin [6,26%]. Also the X-conversion was substantially higher at 6,26 % kaolin added [85 %], compared to 31 % for the 'pure' fuel.

Chemically, water-soluble and total [K], [Cl] and [Si] in the deposits decreased, when increasing the Kaolin doze [0→6,26 %]. This effect was especially strong for water-soluble [K]. In the case of fly ash/aerosols water-soluble and total [K], [Ca] and [Cl] decreased.

[Al] increased in both deposit and flyash/aerosols.

XRD Analysis:

The XRD analyses revealed significant levels of K2SO4 and CaSO4 especially on the downstream side of the deposits, indicating deposition of small particles via eddy vortex formation on the back side of the deposition probe. On the upstream side of the tubes also several cases of identification of SiO2 were seen.

There is not much indication of mineral phases origination from either kaolin or one of the two CFAs tested as additives in the XRD-analyses.

SEM Analysis:

The SEM analyses conducted only on ashes/deposits from wheat straw firing, indicated – as is also obvious on the probe images shown in this report – a very porous structure of upstream deposits. Particles of many different shapes are identified in these deposits.

Only very low levels of Cl is found by SEM-EDX, while some of the individual particles analyzed (by point analysis) showed a significantly higher [K], than what was found in the average chemical composition.

The filter samples consisted mainly of small particles, ~ 2 µm, containing significantly higher concentrations of K, S and Cl, than what was found in the deposits.

Part II:

Additional Work: Performance of Fuels in a Laminar Flow Combustor – NOx formation and Slagging Propensities

1. Abstract

The combustion work carried out by ECN part of TNO further confirms the fuel quality improvements achieved through upgrading (washing and dry torrefaction) during live combustion tests, representing realistic conditions experienced in industrial PF furnaces, decreasing the uncertainty related to the discussed considerations based on fuel indexes calculation results, already presented in D2.3.

2. Biomass materials

Four low-grade biomasses – road side grass, miscanthus, wheat straw and spruce bark were used in this study. The biomass materials were chosen based on their availability and potential energy application. They all originated from The Netherlands, except spruce bark, which originated from Finland. A more complete description of the biomasses including full characterization is given in D2.3.

3. Results and discussion

The methods used in the fuels preparation are fully described in D2.3 and in ref [1,2]. The combustion equipment used in this work (the LCS) simulates real PF burning conditions and its principle of operation is given elsewhere [2]. A schema of the installation is given in Figure 41

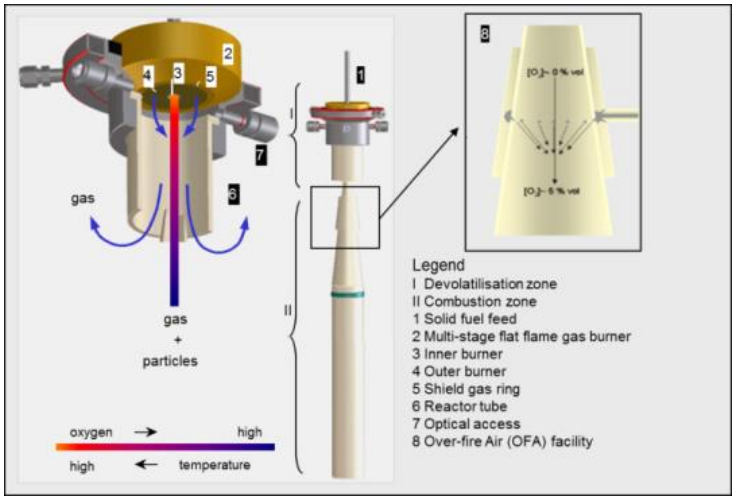

Figure 41: Staged flat flame gas burner and reactor (drop) tube in the lab-scale combustion simulator (LCS).

For this work, the burner was operated with a primary lambda of 0.85 and a total lambda of 1.15 without further (deep) staging. The local gas temperature was slightly above 1400°C. For conversion kinetics, burnout/ash and aerosol formation studies, particle and flue gas samples can be obtained at residence times between 10 and 3000 ms, employing a vertically adjustable, oil-cooled probe. The particles are rapidly cooled and are collected using a cascade impactor. The latter instrument was used for aerosol formation studies. Fly ash samples were taken isokinetically employing a Pilat Mark V cascade impactor using 11 stages (2.8-28 L/min configuration), under combustion conditions with residence time of approximately 2 s. Nuclepore® polycarbonate substrates were used as particle impaction surfaces. For slagging

tests a vertical specialized deposition probe is used. Coupons of ceramic alumina were attached to the probe head to simulate deposition surfaces near burner conditions (burner distance of 280 mm, corresponding to a residence time of approximately 200 ms). The coupons can be removed for further testing (e.g., corrosion) and chemical or microscopic analysis of the deposit. Fouling studies were also carried out by means of a horizontal deposition probe (HDP), which can be placed at a fixed distance from the burner. The HDP is used to mimic the gas/particle flow around a single boiler tube. It is equipped with a ring-shaped quadruple heat-flux sensor assembly and a detachable deposition substrate. While the sensor yields on-line data on the influence of the deposit on the effective heat flux through the tube wall, the tubular substrate is used to collect samples for off-line deposit morphology and chemical composition studies (by means of visual/electron microscopy, also in combination with EDX analyses).

NOx formation

The measured NO_X formation of the untreated and upgraded fuels are shown together with the values of a reference coal in *Figure 42*. The absolute amounts of NO_X formed per unit mass of fuel are specific to the air staging conditions applied in the LCS. For the values shown below, burner staging with a primary lambda of 0.85 and a total lambda of 1.15 without further (deep) staging was applied. Hence, the reported values are specific for these conditions. The measurements were carried out in a two-step procedure. First, gas/particle samples were taken at a short burner distance at which devolatilisation and subsequent volatile matter conversion was completed, yielding a NO_X concentration that is referred to primary NO_X in the following. In the second step, the measurement is repeated at a longer burner distance where char conversion is essentially completed and the final NO_X concentration after conversion is recorded. By subtracting the NOx formed by the gas flame (without solid feed) and performing mass balances for NO_X in the reactor, the secondary NO_X originating from char-bond nitrogen was calculated by subtracting the primary NO_X formed from the final NO_X. Then the total masses of NO_X (primary and secondary) were referred to the total mass of fuel fed during the experiments. By presenting the data in this way, it is possible to make a distinction between primary NO_X generated during the combustion of volatiles and secondary NO_X formed during char combustion, assuming that the volatile-N conversion is much faster than the char-N conversion during the pyrolysis and volatile combustion step, during which the primary NO_X value was determined. With this distinction, it is possible to estimate the potential of further (deep) air staging, since this technique offer the possibility to further reduce primary NO_X.

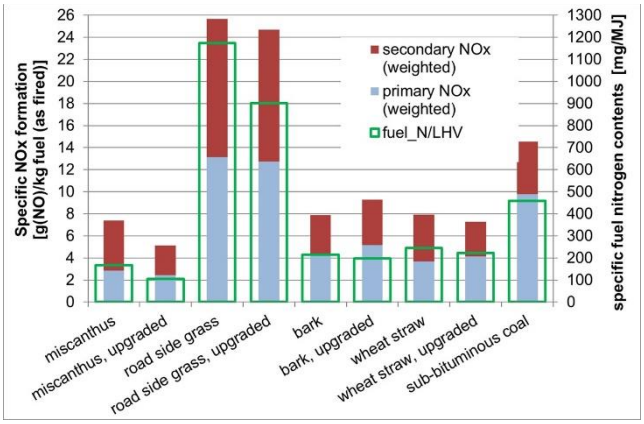

Figure 42: Specific fuel nitrogen content and specific NOX formation: Primary NOX – formed during volatiles combustion; Secondary NOX – formed during char combustion.

As expected, the road side grass samples formed the highest specific NO_X. On the other hand, these samples also show the highest potential of absolute primary NO_X reduction since the road side grass samples form the highest (total) amount of primary NO_X which can be

significantly reduced by air staging techniques , effectively reducing the primary NO_X formation. Nevertheless, it seems unlikely that road side grass can lead to direct NO_X reduction when co-fired with coal because of the large amount of secondary NO_X formed during char combustion that even exceeds the secondary NO_X formed by the reference coal shown in Fig. 2, unlike the other fuels under investigation. Moreover, if road side grass is to be combusted stand-alone, it seems that secondary measures for NO_X reduction, such as SCR or SNCR systems, have to be implemented to ensure compliance with legal limits. These observations are in line with the findings from other works [3] For all the other biomasses NO_X formation seems not to be a problem and the general effect of upgrading is a decreasing tendency for NO_X formation with the exception of spruce bark.

Upgraded miscanthus yielded the lowest specific LCS NO_X formation. The latter is in line with the specific nitrogen content of the fuel. According to the specific nitrogen contents of spruce bark and wheat straw, one would expect that upgraded spruce bark produces slightly less NO_X than upgraded wheat straw. However, the opposite is the case. While the original fuels produce similar amounts of primary NOX, upgraded spruce bark produces significantly more secondary NOX, which is probably due to differences in nitrogen species in the fuels, as well as, to different distribution of volatile-N and char-N [4 Moreover, the higher fuel-Ca content, which was increased after upgrading, can only partially explain this behavior, since Ca is known to catalyze NOX formation reactions, but at lower temperatures [5,6]. Overall, it can be seen that the specific nitrogen content of a fuel gives indications on how the fuel will perform but the total NOX formation is also strongly influenced by other fuel-specific parameters as mentioned above. A more complete study on NOX formation can be found here [7].

Submicron particles formation

Fly ash samples were analyzed for the particle size distribution. The purpose of these measurements was to investigate the impact of pre-washing and torrefaction on the formation of sub-micron particles (aerosols) that can cause fouling and corrosion problems and can affect the operation of electrostatic precipitators and flue gas cleaning in thermal power plants [8]. The latter is particularly true when the aerosols are formed by homogenous nucleation of alkali salt vapors in the flue gas and the release of very fine CaO particles [9,10]. In grass and straw like materials, usually the aerosol formation is dominated by K compounds, namely KCl. If S is present in the fuel, KSO_4 is formed preferentially and the Cl remains mainly in the gas phase as HCl and not in the deposits in the heat transfer surfaces, reducing the high temperature corrosion risk. Other possible aerosol species are K phosphates and carbonates. Since large amounts of alkalis and chlorine are removed during upgrading, it is expected that a significant reduction in fine particulate matter formation can be observed.

Table 13 gives an overview of the achieved fine particulate emission reduction by upgrading. After upgrading, sub-micron particles of spruce bark and miscanthus can be reduced by approximately 37 and 54% by mass, respectively, while the emissions of straw and grass can even be reduced by approximately 69 and 87%, respectively. These values are very promising given that fine particulate fouling problems are a big concern when firing fast growing biomass. The aerosol formation of upgraded spruce bark is less pronounced than for the other samples. The reason for the lower reduction in case of spruce bark is that woody biomass forms predominantly sub-micron particles composed of calcium oxide, originating from the combustion of calcium oxalate. Since calcium oxalate is hardly water-soluble, it was not removed during the pre-washing step. Further analysis of the chemical composition of the individual cascade impactor stage samples could shed light into the nature of the particulate matter.

Table 13: Reduction of sub-micron particles formation after upgrading, expressed as mass per fuel energy input (percentage of initial formation).

Biomass material	Cumulative mass of submicron particle formation (g/GJ)	Submicron particles formation reduction (%)
straw	57.1	-
straw upgraded	17.8	68.8
miscanthus	33.4	-
miscanthus upgraded	15.2	54.5
bark	21.8	-
bark upgraded	13.8	36.7
grass	129.0	-
grass upgraded	18.0	86.0

Fouling

These fuels profit greatly from the potassium removal during the pre-washing. Only spruce bark showed a marginal fouling propensity decrease after pre-washing. Fouling studies were carried out by means of a horizontal deposition probe (HDP), which was placed at a fixed distance from the burner corresponding to a residence time of approximately 2.5 s. The metal surface of the probe was kept at 540 °C, by air cooling. An example of a typical fouling deposit is given in *Figure 43*. The fouling factor, as measured with this probe, is also depicted in *Figure 43* for the four biomass samples and the respective four upgraded materials.

Among the four original untreated materials, wheat straw showed the highest fouling tendency followed by the road side grass. The specific fouling factor (taken as the slope of the straight lines in *Figure 43*) of untreated wheat straw was roughly two times higher than the one of road side grass. This is surprising considering that the grass produced a higher load of submicron particles and has a higher alkali index. Both miscanthus and spruce bark showed equally lower level of fouling tendency.

As confirmed during the submicron particle measurements the fouling tendency is significantly decreased after the removal of the alkalis in the washing step. Except for the bark that showed a neutral behavior, all the other biomasses presented a decrease in specific fouling factor after the upgrading process. In the case of road side grass, the upgrading process contributed to a decrease in the specific fouling factor of about six times and for wheat straw the effect was a benefit of a twofold decrease.

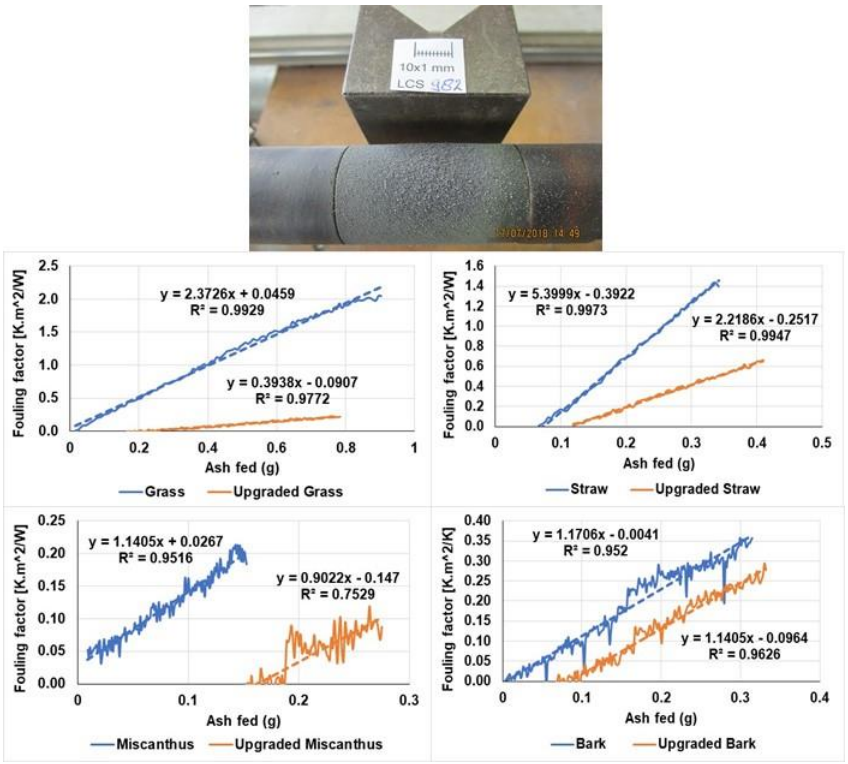

Figure 43: Fouling sample and the fouling factor measurements of the investigated fuels. (metal surface T = 540 °C).

High temperature chlorine corrosion

High temperature chlorine corrosion is mostly due to the presence of Cl in the deposits formed on the heat transfer surfaces [11, 12] as simulated in the HDP measurements used for the fouling propensity determination and directly related to the fuel composition and chemical reactions that take place involving the alkalis, Cl, S, aluminosilicates and the total amount of fly ash particles created during conversion. The chlorine reduction both due to pre-washing and torrefaction yields for wheat straw and miscanthus very similar specific chlorine contents of 30 and 22 mg/MJ, respectively, while spruce bark yields a very low value of 4 mg/MJ of specific chlorine content. Even the very chlorine rich road side grass yields a value of 69 mg/MJ after upgrading. Obviously, these high removal yields are due to the fact that chlorine is mostly present in water-soluble form and can hence be removed efficiently. The achieved values indicate that high temperature chlorine corrosion is expected to be significantly reduced for the upgraded materials. However, the Cl content of the upgraded road side grass can still pose a moderate risk of high temperature chlorine induced corrosion.

The cross section of the deposits of the fouling tests were analyzed by SEM/EDX and the results of the tests carried out with the road side grass, as well as the upgraded road side grass are depicted in Figure 44 and Figure 45. The road side grass was selected for this analysis because it represented the worst case scenario in terms of expected high temperature corrosion and confirmed the benefits of the higher Cl and alkali removal during upgrading. The metal substrate surface can be easily recognized in the elemental mapping of the substrate – by Cr (blue) and Ni (pink), shown in the bottom right part of Figure 44 and Figure 45. The substrate/deposit interface can be seen in the bottom part of each individual picture right above the rich Cr and Ni zone. The composition of the deposit could be roughly evaluated and is also presented. The deposit of the upgraded grass (Figure 45) is depleted in Cl and K when compared to the deposit composition of the original grass (Figure 44), as expected. However, the major difference can be found on the interface of the metal surface. In case of the untreated grass (Figure 44), a thin layer of K associated also with Cl has developed on the surface of the metal substrate, either due to direct condensation of KCl vapors, or deposition of the potassium

chloride aerosols. The latter phenomena are the major mechanisms to promote high temperature chlorine corrosion at the surface of heat exchangers. On the contrary, in the case of upgraded grass, such thin layer of K and Cl is completely absent indicating a significant reduction in the potential for high temperature corrosion. Nevertheless, even after upgrading, still some Cl was found at some located spots at the metal surface and therefore high temperature chlorine corrosion cannot be completely ruled out.

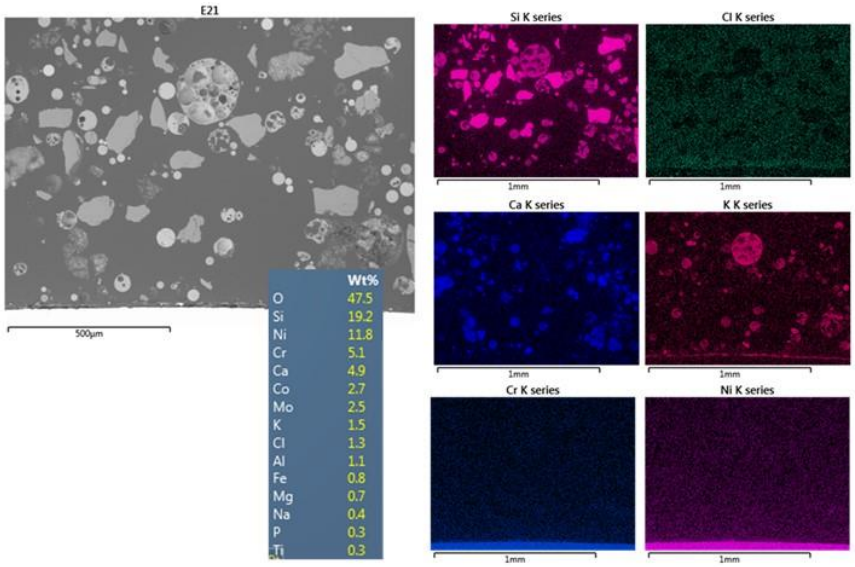

Figure 44: SEM/EDX analysis of the cross section cut of the substrate fouling deposit obtained with the road side grass.

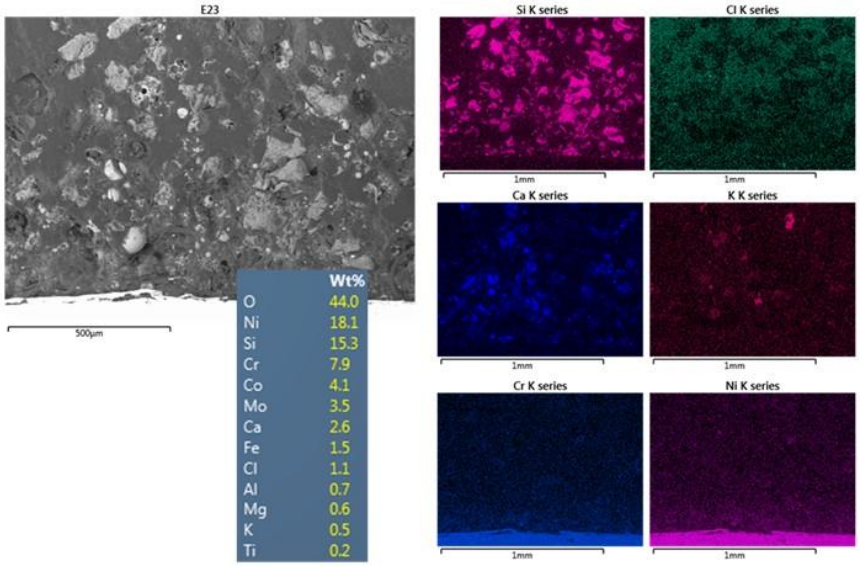

Figure 45: SEM/EDX analysis of the cross section cut of the substrate fouling deposit obtained with the upgraded road side grass.

Near-burner slagging

Slagging tendencies of fuels are often assessed by fuel indices and indicators, often derived for fossil fuel ash. However, they often fail to predict the true slagging propensities of the biomass fuels since the occurrence of specific phases and minerals containing problematic elements are not accounted for [13]. Therefore, live combustion deposits under conditions resembling near-burner environments were carried in order to shed light into the true nature of deposit formation of the fuels under investigation.

Photographs of wheat straw slagging samples taken with the vertical deposition probe, both with untreated and upgraded materials, are shown in *Figure 46*. Both fuels created a rather fluffy, highly sintered deposit that was growing several millimeters in height. The deposit of the upgraded wheat straw appears to be slightly darker in color than the untreated material, which is probably due to a different deposit morphology. The two deposits were further analyzed by SEM/EDX analysis in order to shed light into the morphology and the composition of the deposits. The SEM magnification of the untreated and upgraded wheat straw deposits is presented in Fig. 6. Even though the morphology does not differ strongly, it can clearly be seen than the deposited particles from the upgraded wheat straw are finer than from the untreated material. The latter allows for a denser packing of the particles which in turn explains the darker color of the deposit. Also under this magnification it is clearly visible that individual particles are sintered together and form a porous solid network, i.e. no molten slag is formed. The chemical composition of selected regions of the deposits is given in *Figure 46*. The SEM/EDX analysis reveals that the composition of the deposits is fairly homogeneous for both samples. The most remarkable difference is the reduction in potassium by roughly 50% in the deposit of the upgraded wheat straw sample, which was anticipated due to the pre-washing. It appears that calcium silicates form the basis for the sintering of the particles, while glass-type alkali silicates appear to play a minor role. Overall, it can be concluded that pre-washing of wheat straw has minor effect on the slagging propensity of the feedstock. However, for none of the two cases molten, running slag could be observed so the slagging risk for the fuels should be considered moderate.

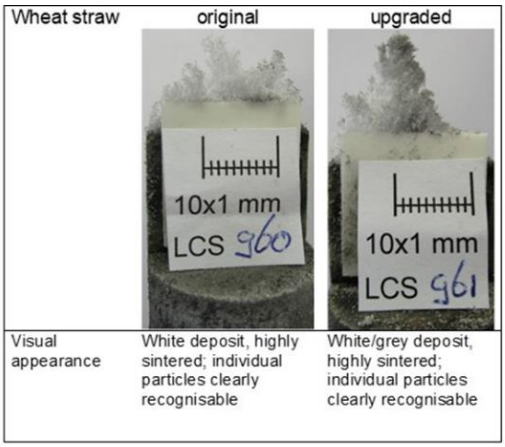

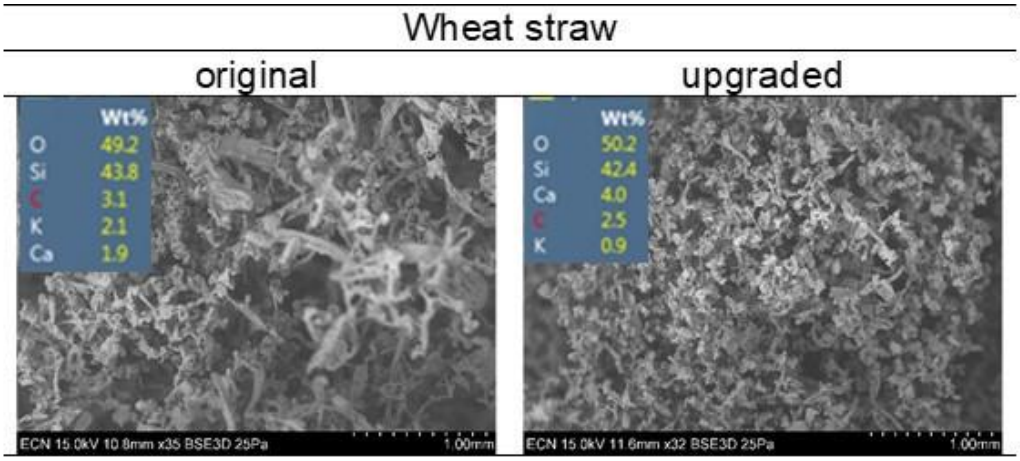

Figure 46: 6 Photographs and SEM/EDX analysis of wheat straw slagging deposits.

The deposits collected with the untreated and upgraded miscanthus differ visually little from the ones collected from wheat straw. They appear very fluffy, consisting of highly sintered individual particles (*Figure 47*). Like for the wheat straw case, also the upgraded miscanthus deposit is darker in color and significantly larger in size compared to the untreated material. However, when taking a look at the SEM magnifications (*Figure 47*), distinct differences compared to the wheat straw deposits are visible. In case of miscanthus, more molten particles are observable. Nonetheless, also untreated and upgraded miscanthus form a solid porous network of sintered particles, i.e. no running slag is formed. Interestingly, also the upgraded miscanthus forms a deposit that is made up of significantly finer material than the untreated feedstock. The underlaying reasons for this difference in morphology are yet to be investigated. Most probably the silica based skeleton of the original materials is desegregated into smaller size particles during the thermal treatment in the torrefaction step. Therefore, smaller silica based particles must be impacting and building up a deposit with a more packed slag layer, in the case of these particular torrefied materials.

Miscanthus	original	upgraded
		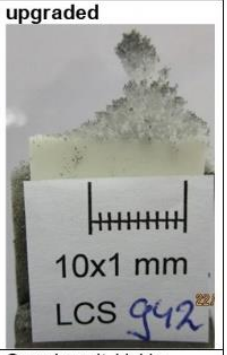
Visual appearance:	White deposit, highly sintered; individual particles clearly recognisable	Grey deposit, highly sintered; individual particles clearly recognisable

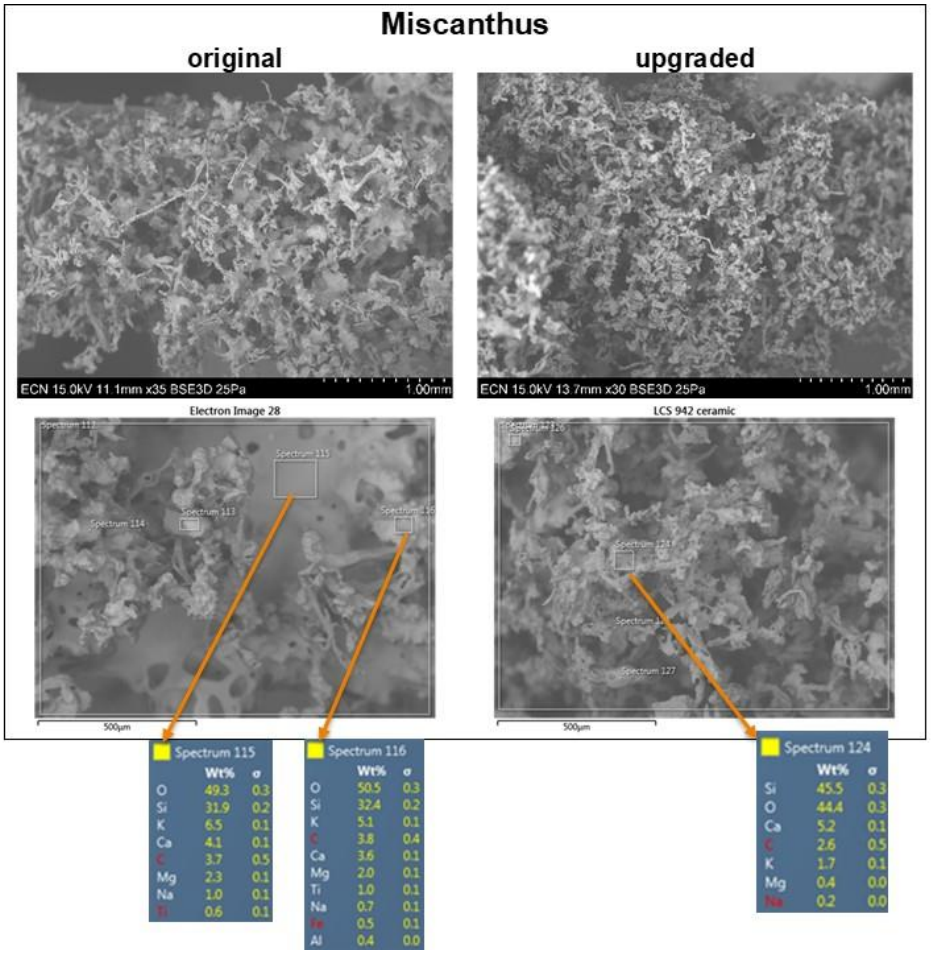

Figure 47: Photographs and SEM/EDX analysis of miscanthus slagging deposits.

Magnifications of the SEM micrographs of the miscanthus deposits are given in Figure 47. Only with the higher magnification the true extent of melting can be visualized. In case of untreated miscanthus completely molten particles made up of alkali and calcium silicates (see EDX spectra 115 and 116 in Figure 47) were found in the deposit. The partially molten particles of upgraded miscanthus are made up of calcium silicates with significantly lower concentrations of potassium. The latter is most likely the reason for the higher melting temperatures of the ashes. Pre-washing of miscanthus results in a reduced slagging propensity because the fully molten particles are expected to form a higher risk, despite the increased height of the deposit created with upgraded miscanthus. Nonetheless, also upgraded miscanthus still exposes a moderate slagging risk.

Photographs of the collected slagging samples produced of road side grass are given in Figure 48. The untreated road side grass formed a fully molten deposit, while the upgraded material created a highly sintered deposit in which individual particles are still visible. Evidently, the visual impact of pre-washing is the strongest for the road side grass if the slagging propensity is concerned.

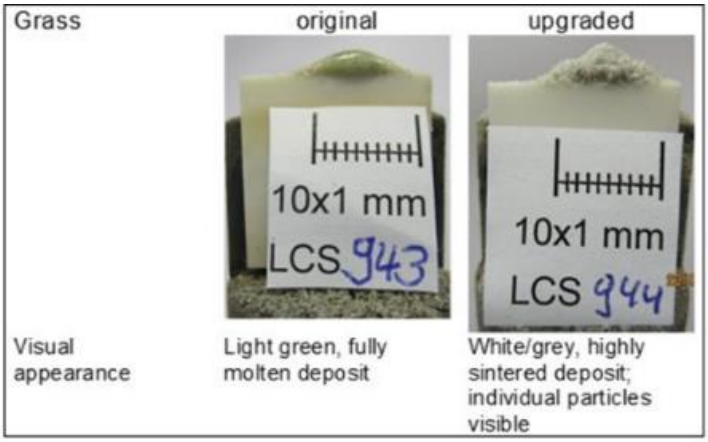

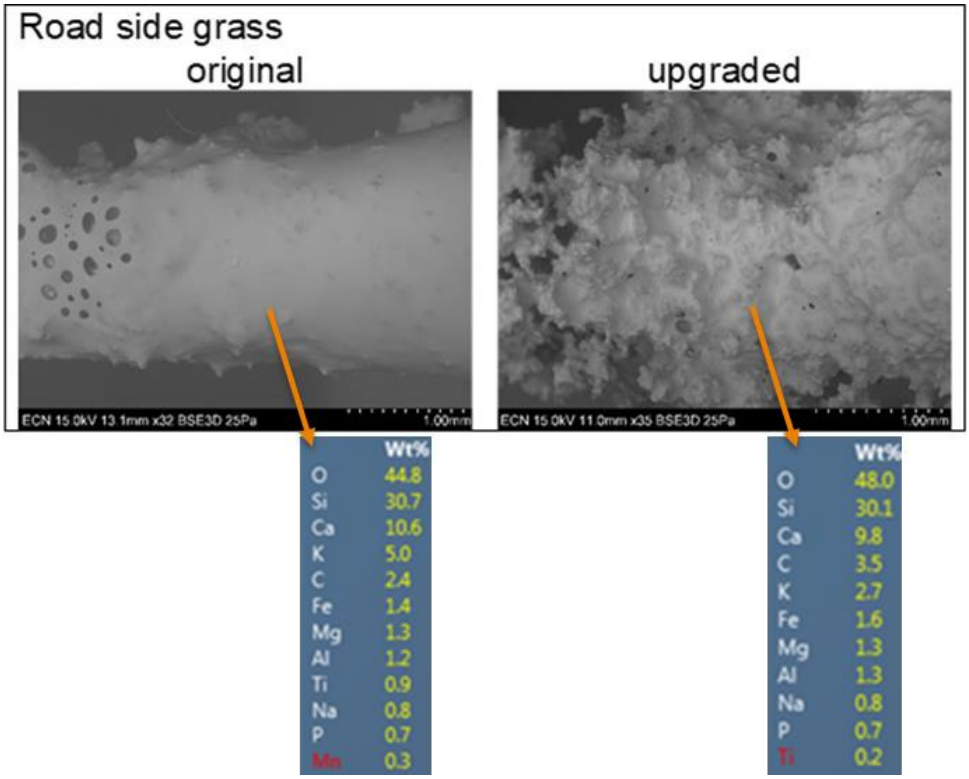

Figure 48: Photographs and SEM/EDX analysis of roadside grass slagging deposits.

However, the SEM micrographs reveal that the improvement with upgraded road side grass is not as promising as expected from the visual inspection. The top layer of the deposit, where temperatures are the highest, shows initial melting of the material (Figure 48). The SEM/EDX micrographs of the deposits of roadside grass offer insight into the chemical composition. The molten deposit of untreated road side grass is very homogeneous and is made up of calcium silicates with sizeable amounts of potassium. The trapped particles are either sand or calcium oxide units originating from limestone present in the fuel. The composition of the deposit of the upgraded material differs only marginally from the untreated one with the exception of a halved potassium concentration. The latter underlines the fact that only small alterations of potassium content can have measurable impact on the melting behavior of an ash. Overall it can be

concluded that both road side grass samples expose a severe slagging risk when fired in a pulverized fuel installation.

Spruce bark	original	upgraded
		
Visual appearance	Black/brown, loose deposit; no sintering visible	Black/brown, loose deposit; no sintering visible

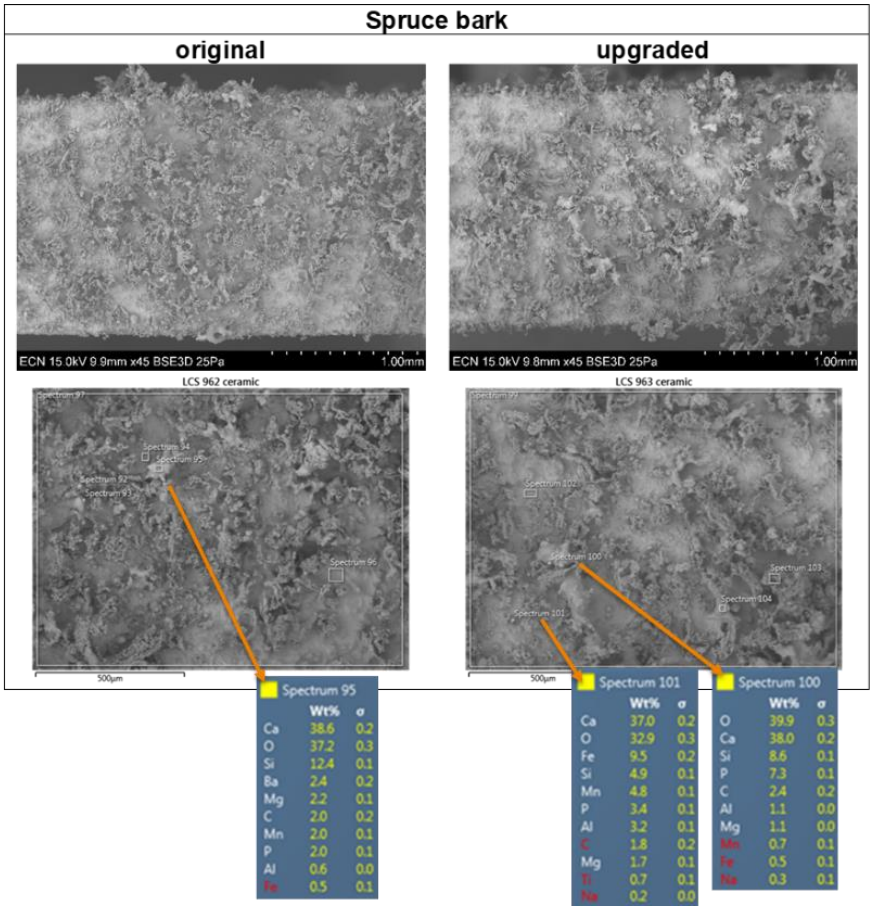

Figure 49: Photographs and SEM/EDX analysis of spruce bark slagging deposit

The case of spruce bark is completely different from the other biomasses tested. Unlike the other fuels under investigation, both untreated and upgraded spruce bark formed a loose black-brown deposit with no signs of sintering or melting, at least not visible with the naked eye, as depicted in Figure 49. Also the SEM micrographs in Figure 49 reveal that only loose deposits are formed with few partially molten particles. Overall, the deposit morphologies resemble the ones seen for wood firing in earlier tests carried out at ECN part of TNO. In case of spruce bark, the deposit chemistry is dominated by calcium containing species, mainly calcium oxide, which explains why only very little material was deposited, because the melting point of calcium oxide is very high. Those few particles that are partially molten generally show enriched silica

contents, but also enrichments of phosphorous and/or iron and manganese, see EDX spectra 95, 100 and 101 in Figure 49. Those elements, in particular silica and iron are prone to form lower melting eutectics with calcium which explains the partially molten nature of the particles. Composition wise, the two deposits differ overall mainly in the calcium content, which is approximately 2%-wt. lower for the upgraded sample. The latter is most likely due to the partial removal of calcium during the pre-washing step. Overall, the two materials can be considered to expose a low slagging risk for boiler operation.

4. Conclusions

The combustion results showed a general decrease in NOx formation after upgrading; High temperature chlorine corrosion can be effectively mitigated; Fine particulate matter (submicron/aerosols) formation is strongly reduced, effectively reducing the risk of alkali induced fouling. However, slagging tests revealed that pre-washing and torrefaction has minor impact on the slagging propensity of the fuel. Only, slightly reduced slagging is observable and therefore the use of mineral combustion additives, or smart blending with other fuels in order to further mitigate the slagging risks is strongly recommended.

References

Part I:

Damø, A.J. ; Jensen, P.A. ; Frandsen, F.J.; Wu, H. ; Glarborg, P.; *Fly Ash Formation during Suspension-Firing of Biomass. Effects of Residence Time and Fuel-Type*; Energy & Fuels, 31(1), 555–570, 2017.

F. J. Frandsen; Ash Formation, Deposition and Corrosion When Utilizing Straw for Heat and Power Production; Doctoral Thesis, Technical University of Denmark, ISBN-9788792481405, 2011.

Frandsen, F.J.; *Quantification of Release of Critical Elements, Formation of Fly ash and Aerosols: Status on Current Understanding and Research Needs*; Proc. INFUB11, Albufeira, Algarve, Portugal, April, 18-21, 2017.

Hein, K.R.G.; *Sustainable Energy Supply and Envionment Protection – Strategies, Resources and Technologies*; In: R. Gupta, T. Wall, M. Hupa, F. Wigley, D. Tillman, F.J. Frandsen, Proc. Int. Conf. 'IMPACT OF FUEL QUALITY ON POWER PRODUCTION AND THE ENVIRONMENT', Banff Conference Centre, Banff, Alberta, Canada, Sept. 29 - Oct. 4, 2008.

Laxminarayan, Y.; *Formation, Sintering and Removal of Biomass Ash Deposits*; PhD-Thesis, Department of Chemical and Biochemical Engineering, Technical University of Denmark, 2018.

Naimi, S., Funch, J.T.; *The Influence of Aditives on Deposit Formation from Biomass Combustion*; MSc-Thesis, Department of Chemical and Biochemical Engineering, Technical University of Denmark, 2019.

Wang, G.; *Potassium Capture by Kaolin and Coal Fly Ash*; PhD-Thesis, Department of Chemical and Biochemical Engineering, Technical University of Denmark, 2018.

Part II:

[1] P. Abelha, A. Janssen, C. Mourão Vilela, P. Nanou and M. Carbo. Low-Grade Biomass Upgrading by Washing and Torrefaction: Lab and Pilot-Scale Results. 26th European Biomass Conference and Exhibition, (2018) 1209-1220, 14-17 May, Copenhagen, Denmark (3DV.6.3).

[2] P. Abelha, C. Mourão Vilela, P. Nanou, M. Carbo, A. Janssen and S. Leiser, Combustion improvements of upgraded biomass by washing and torrefaction. Fuel 253 (2019) 1018–1033.

[3] F. Hensgen, L. Bühl, I. Donnison, M. Frasier, J. Vale, J. Corton, K. Heinsoo, I. Melts, M. Wachendorf. Mineral concentrations in solid fuels from European semi-natural grasslands after hydrothermal conditioning and subsequent mechanical dehydration. Bioresource Technology 118 (2012) 332–342.

[4] P. Abelha, I. Gulyurtlu, I. Cabrita. Release Of Nitrogen Precursors From Coal And Biomass Residues in a Bubbling Fluidized Bed. Energy & Fuels, 2008, 22 (1), 363–371.

[5] M. Y. Yao & D. F. Che. Catalytic Effects of Minerals on NOx Emission from Coal Combustion. Energy Sources, Part A: Recovery, Utilization, and Environmental Effects, (2007), 29:11, 1005-1016.

[6] Z. Zhao, W. Li J. Qiu, X. Wang, B. Li. Influence of Na and Ca on the emission of NOX during coal combustion. Fuel (2006), 85, 601-606.

[7] F. Van Dijen. Modelling primary NOX and primary N2O of pulverised fuel combustion and circulating fluidised bed combustion, VGB Powertech, VGB-B 15, Essen, Germany, 2018.

[8] F. Mylläri, P. Karjalainen, R. Taiplae, P. Aalto, A. Häyrinen, J. Rautiainen, L. Pirjola, R. Hillamo, J. Keskinen, T. Rönkkö, Physical and chemical characteristics of flue-gas particles in a large pulverized fuel-fired power plant boiler during co-combustion of coal and wood pellets, Combustion and Flame 176, (2017) 554-566.

[9] Ulrich Kleinhans, Christoph Wieland, Flemming J. Frandsen, , Hartmut Spliethoff. Ash formation and deposition in coal and biomass fired combustion systems: Progress and challenges in the field of ash particle sticking and rebound behavior. Progress in Energy and Combustion Science 68 (2018) 65-168.

[10] K. V. Shah, M. K. Cieplik, C. I. Betrand, W. L. van de Kamp, H. B. Vuthaluru. Correlating the effects of ash elements and their association in the fuel matrix with the ash release during pulverized fuel combustion. Fuel Processing Technology 91 (2010) 531–545.

[11] Y. Niu, H. Tan, S. Hui, Ash-related issues during biomass combustion: Alkali-induced slagging, silicate melt-induced slagging (ash fusion), agglomeration, corrosion, ash utilization, and related countermeasures. Progress in Energy and Combustion Science 52 (2016) 1-61

[12] H.P. Michelsen, F. Frandsen, K. Dam-Johansen, O.H. Larsen, Deposition and high temperature corrosion in a 10 MW straw fired boiler, Fuel Processing Technology 54 (1998) 95-108

[13] S.V. Vassilev, D. Baxter, C.G. Vassileva, An overview of the behaviour of biomass during combustion: Part II. Ash fusion and ash formation mechanisms of biomass types, Fuel 117 (2014), 152-183